Collective and two-quasiparticle excitations in ^{128}Te

S. F. Hicks,[1,*] J. C. Boehringer,[1] N. Boukharouba,[2,3] C. Fransen,[2,4] S. R. Lesher,[2,5] J. M. Mueller,[6] J. R. Vanhoy,[6] and S. W. Yates[2,7]

[1]*Department of Physics, University of Dallas, Irving, Texas 75062, USA*
[2]*Department of Physics and Astronomy, University of Kentucky, Lexington, Kentucky 40506-0055, USA*
[3]*Department of Physics, University of Guelma, Guelma 24000, Algeria*
[4]*Institut für Kernphysik, Universität zu Köln, Zülpicher Strasse 77, D-50937 Köln, Germany*
[5]*Department of Physics, University of Wisconsin-La Crosse, La Crosse, Wisconsin 54601, USA*
[6]*Department of Physics, United States Naval Academy, Annapolis, Maryland 21402, USA*
[7]*Department of Chemistry, University of Kentucky, Lexington, Kentucky 40506-0055, USA*

(Received 17 May 2012; revised manuscript received 5 August 2012; published 15 November 2012)

Excited levels of ^{128}Te to 3.3 in MeV excitation have been studied using γ-ray spectroscopy following inelastic scattering of accelerator-produced neutrons. Spectroscopic information, including transition energies, level spins, $E2/M1$ multipole-mixing ratios, and γ-ray branching ratios, was determined from γ-ray excitation functions measured from $E_n = 2.15$–3.33 MeV in 90-keV increments, γ-ray angular distributions measured at $E_n = 2.2$, 2.8, and 3.3 MeV, and $\gamma\gamma$ coincidences measured at $E_n = 3.6$ MeV. Lifetimes of levels in ^{128}Te were deduced using Doppler-shift attenuation techniques. Absolute transition probabilities were determined for many levels and compared to interacting boson model and particle-core coupling model calculations to identify few particle and collective structures; states exhibiting the decay characteristics expected for two-phonon, mixed-symmetry, and quadrupole-octupole coupled states are identified.

DOI: 10.1103/PhysRevC.86.054308 PACS number(s): 25.40.Fq, 23.20.−g, 27.60.+j, 21.60.−n

I. INTRODUCTION

The structure of tellurium nuclei has been the subject of many investigations [1–35]. The ratio of $E(4_1^+)/E(2_1^+)$ ranges between 1.94 and 2.09 for the even-even $^{114-130}$Te isotopes, which is very near the harmonic vibrational value of two, and the energies and decay characteristics of the lowest 2_1^+ and 3_1^- states in these nuclei are characteristic of quadrupole and octupole phonons, respectively [2]. The observation of such well-defined, phonon structures at low excitation energies has led to the prediction of higher-lying collective structures, including mixed-symmetry (MS) excitations, in which the neutron and proton contributions are distinguishable [36], and quadrupole-octupole coupled (QOC) excitations formed by the coupling of the normal one-phonon 2_1^+ and 3_1^- states [37].

Previous investigations of collective excitations in the even-even Te nuclei have revealed a fragmentation of the lowest $2_{1,\mathrm{MS}}^+$ one-phonon MS strength in $^{122-130}$Te [19,33] and also in the dipole two-phonon MS and normal collective excitations in $^{122-126,130}$Te [23,25,28]. The fragmentation observed in the dipole excitations is considerably greater than predicted by quasiparticle-phonon model (QPM) calculations and is indicative of the Te nuclei exhibiting features of moderately deformed nuclei [28].

In addition to its importance for investigating collective nuclear excitations, ^{128}Te is one of only a handful of nuclides in which double β decay has been identified [38–40]. Nuclear matrix elements connecting initial and final states are important input for calculating double β-decay rates and current model calculations are not in agreement [41]. Detailed nuclear structure information on low-spin states in ^{128}Te may prove helpful in constraining these calculations.

To investigate collective and few-particle structures in ^{128}Te and to provide detailed structural information on low-lying levels, especially level lifetimes important for both nuclear model comparisons and double β-decay calculations, a series of measurements using γ-ray detection following inelastic neutron scattering has been performed. The experimental techniques and data reduction procedures used in these $(n,n'\gamma)$ measurements are discussed in Sec. II; level properties of states requiring special attention are given in Sec. III; model calculations along with experimental comparisons are the topic of Sec. IV; and special collective and few-particle structures are discussed in Sec. V. Finally, our conclusions are presented in Sec. VI.

II. EXPERIMENTAL METHOD AND DATA ANALYSIS

Measurements were performed using the neutron production and γ-ray detection facilities at the University of Kentucky 7 MV electrostatic accelerator laboratory (http://www.pa.uky.edu/accelerator/). The ^{3}H$(p,n)^3$He reaction was used to produce monenergetic neutrons. The sample used for all singles measurements consisted of two nonuniform ingots isotopically enriched to 98.08% in ^{128}Te. The two ingots were placed together in a nearly cylindrical configuration and enclosed in a sealed plastic bag. The "diameter" of the scattering sample was 2.2 cm in one direction and 1.5 cm in the other, while the height of the sample was 4.3 cm. Suture thread was used suspend the sample.

γ-γ coincidences were measured at an incident neutron energy of 3.6 MeV. Neutrons emerging from the

*Electronic address: hicks@udallas.edu

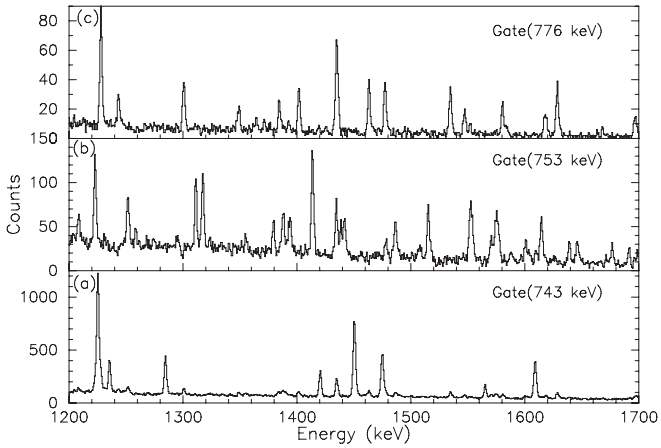

FIG. 1. Portion of the coincidence spectra from gates set on the (a) 743-keV, (b) 753-keV, and (c) 766-keV γ rays from the first, second, and third excited states of ^{128}Te, respectively.

tritium-containing gas cell were formed into a 1-cm "beam" by a lithium-loaded collimator approximately 75 cm in length. The experimental arrangement is discussed in detail in Ref. [42]. A natural Te sample was hung coaxially with the beam, and four 50% to 55% efficiency high-purity germanium (HPGe) detectors were placed in a coplanar arrangement approximately 6 cm from the center of the sample. Data were stored in event mode, and a two-dimensional matrix was constructed off line by considering pairwise coincidences. Portions of gated coincidence spectra are shown in Fig. 1.

γ-ray singles measurements were used to measure γ-ray excitation functions, angular distributions, and Doppler shifts. γ rays were detected with a Compton-suppressed n-type HPGe detector with 51% relative efficiency and an energy resolution of 2.1 keV full width at half maximum at 1.33 MeV. Compton suppression was achieved using a BGO annular detector surrounding the HPGe detector. The gain stability of the system was monitored using ^{226}Ra and ^{152}Eu radioactive sources. The neutron scattering facilities, time-of-flight neutron background suppression, neutron monitoring, and data reduction techniques have been described elsewhere [42,43].

γ-ray excitation functions were measured at incident neutron energies between 2.15 and 3.33 MeV in approximately 90-keV steps. The thresholds and shapes of the excitation functions were used to identify new levels and to place γ rays in the level scheme. For example, the differences in thresholds of the two γ rays shown in the bottom two panels of Fig. 2 show clearly that the 323.5- and 636.3-keV γ rays do not originate from the same level. Close examination of the excitation function for the latter reveals a second threshold arising from feeding from the 2456.7-keV level by the 323.5-keV γ ray. The shapes of the excitation functions can also contribute to the determination of level spins, as can the angular distributions, as discussed below. In this procedure, the yields from the γ-ray excitation function measurements were corrected for γ-ray detection efficiency and were normalized to yields from the neutron monitor, whose yields were corrected for efficiency as a function of neutron energy to obtain relative γ-ray production cross sections. A normalization appropriate

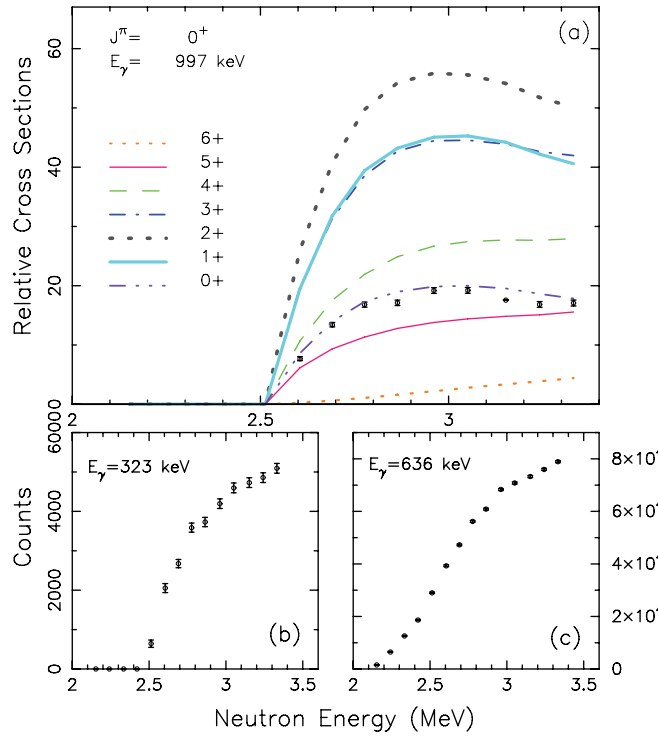

FIG. 2. (Color online) Panel (a) compares the excitation function for the 996.6-keV γ ray from a new 0^+ level at 2516.6 keV with neutron production cross sections from statistical model calculations. The excitation functions for the 323.5- and 636.3-keV γ rays are shown in panels (b) and (c), respectively. These γ rays were adopted [44] as arising from the same level at 2133.3 keV; the excitation functions, in addition to $\gamma\gamma$ coincidence data, show that the former γ ray decays into the 2133.3-keV level.

for interpreting cross sections was obtained by comparing statistical model calculations and experimental cross sections for 0^+ levels. These relative cross sections were then compared to theoretical values calculated with the statistical model code CINDY [45], using optical model parameters for this mass and energy region [46]. The top panel of Fig. 2 shows statistical model calculations compared to experimental data for a new 0^+ level at 2516.6 keV; figures such as this are used to evaluate level spin assignments and branching ratios. Levels to approximately 3 MeV that exhibit inconsistencies with the statistical model calculations are indicated by an m in Table I. Differences between calculations and experimental data indicate either missing decay strength, which affects the branching ratios, or states not adequately represented by a statistical interpretation. γ rays below about 140 keV were not detected because of the limits of the experimental detection efficiency in these measurements and contribute to the missing strength.

γ-ray angular distributions were measured at incident neutron energies of 1.7, 2.8, and 3.4 MeV. Level spins and multipole-mixing ratios can be deduced by comparing the measured angular distributions with calculations from the statistical model code CINDY [45], as discussed previously [31]. Sample γ-ray angular distributions are shown in Fig. 3.

TABLE I. Levels, lifetimes, and level properties in ^{128}Te. When the spin of the initial state is not definite, the mixing ratios and $B(\sigma\lambda)$'s presented are those of the first spin listed. Uncertainties are in the least significant digit(s). Brackets around E_γ indicate a tentative placement. Multipole-mixing ratios with uncertainties that span the entire range of values are noted by *ind*. Weisskopf units are defined in the following way for all tables, $B(E1)_{\text{W.u.}} = 1.636e^2$ fm^2, $B(M1)_{\text{W.u.}} = 1.7905\mu_N^2$, $B(E2)_{\text{W.u.}} = 38.279e^2$ fm^4.

J^π	E_x (keV)	Note	E_γ (keV)	E_f (keV)	BR (%)	$\tan^{-1}(\delta)$	$F(\tau)$	τ (fs)	$B(M1)$ (μ_N^2)	$B(E2)$ (W.u.)
2^+	743.20(5)	a	743.20(5)	0	100			$4780^{+40}_{-40}{}^{r}$		19.7^{+4}_{-4}
4^+	1497.02(7)	a	753.82(5)	743	100					
2^+	1519.96(6)	a	776.73(5)	743	96.9(1)	1.26^{+6}_{-9}	0.023(7)	2400^{+1100}_{-600}	$4.6^{+18}_{-9}\times10^{-3}$	28^{+10}_{-10}
						-0.09^{+12}_{-7}			$4.9^{+17}_{-16}\times10^{-2}$	0.25^{+9}_{-8}
		a	1520.00(9)	0	3.1(1)					$3.4^{+13}_{-12}\times10^{-2}$
6^+	1811.47(23)	a	314.45(22)	1497	100			0.69(4)ns^r		9.8^{+7}_{-6}
2^+,(3^+)	1968.51(7)	a	448.7(3)	1520	0.9(9)		0.160(11)	301^{+25}_{-22}	$\leqslant1.9^{+22}_{-19}\times10^{-2}$	$\leqslant35^{+41}_{-35}$
		a	1225.30(5)	743	99.1(9)	1.32^{+6}_{-6}			$6.3^{+3}_{-3}\times10^{-3}$	24^{+13}_{-8}
						0.13^{+13}_{-7}			$1.0^{+1}_{-1}\times10^{-1}$	0.43^{+5}_{-4}
0^+	1978.95(7)	a	1235.50(5)	743	100		0.027(18)	2040^{+1700}_{-630}		3.6^{+17}_{-17}
4^+	2027.77(6)	a	530.72(5)	1497	60.0(2)	-0.16^{+10}_{-6}	0.097(31)	530^{+270}_{-140}	$4.2^{+16}_{-15}\times10^{-1}$	14^{+6}_{-6}
		a	1284.60(6)	743	40.0(2)					4.6^{+17}_{-16}
5^-	2133.28(12)	a,c	636.26(10)	1497	100	*E*1				
3^+	2163.56(5)	a,d	643.64(5)	1520	41(1)	1.32^{+6}_{-3}	0.067(14)	820^{+230}_{-150}	$6.5^{+27}_{-37}\times10^{-3}$	91^{+68}_{-31}
						0.41^{+13}_{-12}			$9.0^{+22}_{-27}\times10^{-2}$	15^{+5}_{-4}
		a	666.54(6)	1497	24(1)	0.53^{+10}_{-9}			$4.2^{+13}_{-12}\times10^{-2}$	12^{+7}_{-4}
		a	1420.31(6)	743	35(1)	0.41^{+10}_{-6}			$7.1^{+19}_{-19}\times10^{-3}$	$2.5^{+8}_{-7}\times10^{-1}$
2^+	2193.46(7)	a	1450.24(5)	743	91.2(1)	-0.03^{+9}_{-6}	0.461(7)	72^{+2}_{-2}	$2.4^{+1}_{-1}\times10^{-1}$	$3.8^{+2}_{-2}\times10^{-2}$
						1.19^{+6}_{-9}			$3.3^{+10}_{-9}\times10^{-2}$	$3.6^{+11}_{-11}\times10^{+1}$
		a	2193.52(14)	0	8.8(1)					$5.1^{+3}_{-2}\times10^{-1}$
$1^{(+)}$	2217.89(7)	a,c	697.91(29)	1520	5.7(8)	*ind*	0.094(12)	573^{+89}_{-76}	<0.022	<17
		a	1474.66(5)	743	89.3(9)	0.16^{+15}_{-16}			$2.7^{+6}_{-5}\times10^{-2}$	$1.2^{+3}_{-2}\times10^{-1}$
		a	2218.18(25)	0	5.0(3)				$4.5^{+10}_{-8}\times10^{-4}$	
4^+	2270.42(9)	a,m	773.40(6)	1497	100	0.22^{+41}_{-13}	0.189(21)	255^{+41}_{-29}	$4.6^{+8}_{-12}\times10^{-1}$	14^{+5}_{-3}
0^+	2308.25(6)	e,n	788.29(8)	1520	28(2)		0.024(24)	>1.7 ps		<13
		a	1565.05(7)	743	72(2)					<1.0
7^-	2338.51(27)	a,d	526.23(13)	1811	100					
2^+	2352.34(7)	a	1608.88(6)	743	86.8(2)	-0.19^{+10}_{-9}	0.232(11)	198^{+14}_{-10}	$5.8^{+20}_{-6}\times10^{-2}$	$3.1^{+3}_{-10}\times10^{-1}$
		a	2353.25(14)	0	13.2(2)					$2.0^{+2}_{-2}\times10^{-1}$
4^-	2396.69(15)	a	233.24(29)	2164	3.3(3)	*E*1				
		a	263.38(20)	2133	88.1(4)	0.38^{+12}_{-10}				
		a	368.56(27)	2028	8.5(3)	*E*1				
6^+,$(5,4^+)$	2404.9(4)	a,c,v	[593.5(5)]	1811						
		a,v	[907.9(3)]	1497						
4^+,(5^+)	2426.05(9)	a	398.61(24)	2028	10.6(4)	0.56^{+19}_{-47}	0.327(24)	124^{+15}_{-12}	$5.4^{+27}_{-16}\times10^{-1}$	$5.0^{+17}_{-22}\times10^{+2}$
		a	928.99(6)	1497	89.4(4)	-0.13^{+7}_{-6}			$5.0^{+7}_{-6}\times10^{-1}$	3.7^{+5}_{-5}
4,6	2456.74(24)	n	323.46(21)	2133	100					
0^+	2482.19(9)	n	1738.99(7)	743	100		0.171(31)	290^{+80}_{-50}		4.6^{+10}_{-10}
4^+	2487.42(7)	c,n	967.40(14)	1520	18.8(4)		0.114(27)	460^{+160}_{-100}		10^{+3}_{-3}
		a	990.39(8)	1497	42.6(6)	0.41^{+19}_{-22}			$4.6^{+19}_{-16}\times10^{-2}$	3.2^{+14}_{-11}
		a	1744.27(12)	743	38.7(7)					1.1^{+3}_{-3}
3^-	2494.20(7)	c,d,g,n	(526.25(13))	1969	(3.2(4))	*E*1	0.148(13)	340^{+40}_{-30}	$(2.4^{+6}_{-5}\times10^{-4}$W.u.)	
		n	974.21(28)	1520	4.7(2)	*E*1			$6^{+1}_{-1}\times10^{-5}$W.u.	
		a	1751.00(6)	743	92.1(3)	*E*1			$1.9^{+2}_{-2}\times10^{-4}$W.u.	
2^+	2508.14(7)	a,m	1764.88(6)	743	73.5(4)	0.56^{+22}_{-18}	0.101(14)	528^{+91}_{-69}	$1.0^{+3}_{-4}\times10^{-2}$	$4.9^{+20}_{-13}\times10^{-1}$
		a	2508.30(13)	0	26.5(4)					$1.1^{+2}_{-2}\times10^{-1}$
0^+	2516.60(8)	n	996.64(6)	1520	100					

TABLE I. *(Continued.)*

J^π	E_x (keV)	Note	E_γ (keV)	E_f (keV)	BR (%)	$\tan^{-1}(\delta)$	$F(\tau)$	τ (fs)	$B(M1)$ (μ_N^2)	$B(E2)$ (W.u.)
3^+	2550.49(7)	m,n	1030.40(15)	1520	16.3(14)	-1.57^{+19}_{-16}	0.187(29)	259^{+56}_{-41}	$1.2^{+8}_{-8}\times10^{-8}$	12^{+22}_{-16}
		a	1053.46(7)	1497	63.4(3)	0.03^{+6}_{-6}			$1.2^{+3}_{-3}\times10^{-1}$	$3.6^{+7}_{-7}\times10^{-2}$
		a	1807.44(15)	743	20.3(17)	-0.03^{+12}_{-13}			$7.5^{+22}_{-19}\times10^{-3}$	$3.1^{+9}_{-8}\times10^{-3}$
5^-	2571.69(16)	a,c	175.73(29)	2397	12.8(16)	0.06^{+7}_{-15}				
		a	438.05(21)	2133	80.8(21)	-0.38^{+10}_{-6}				
		n	760.16(12)	1811	6.4(17)	*E*1				
(6)	2587.3(3)	n	249.9(6)	2338	23.0(13)					
		a	453.78(23)	2133	77.9(13)					
	2599.2(6)	a,c,d	787.5(5)	1811						
3^+	2630.30(9)	ac	1887.10(7)	743	100	0.56^{+10}_{-6}	0.307(22)	137^{+15}_{-14}	$4.4^{+8}_{-9}\times10^{-2}$	1.8^{+5}_{-3}
	2643.43(12)	a	1900.23(11)	743	100		0.207(45)	230^{+78}_{-120}		
	2655.4(4)	a,c	[843.9(5)]	1811						
		a,d	[1158.3(5)]	1497						
4	2665.30(16)	n	532.02(10)	2133			0.212(149)	220^{+660}_{-120}		
5	2700.95(34)	n	567.67(32)	2133		0.19^{+57}_{-35}				
1	2706.77(9)	a,c	1963.55(7)	743	85.4(6)	0.94^{+56}_{-56}	0.355(63)	115^{+8}_{-8}	$1.9^{+15}_{-16}\times10^{-2}$	3.5^{+330}_{-24}
		a	2706.96(28)	0	14.6(6)				$3.6^{+5}_{-4}\times10^{-3}$	
1(2,3)	2712.40(8)	a	1192.58(32)	1520	11.7(18)	*ind*	0.210(12)	234^{+16}_{-16}	$\leqslant$0.21	$\leqslant$5.4
		a	1969.19(7)	743	88.3(18)	-0.72^{+91}_{-72}			$1.6^{+10}_{-16}\times10^{-2}$	1.2^{+61}_{-7}
	2718.79(14)	n	1221.75(12)	1497						
		n	691.70(71)	2028						
5,(3,4,6)	2736.23(18)	a	602.95(13)	2133						
3	2748.58(6)	e,n	555.24(8)	2193	3.0(10)		0.054(22)	1030^{+760}_{-310}	$\leqslant$0.018	$\leqslant$17
		n	780.24(7)	1969	20.2(12)	-0.28^{+12}_{-16}			$2.2^{+12}_{-11}\times10^{-2}$	1.1^{+7}_{-6}
		n	1228.02(10)	1520	31.7(12)	-0.03^{+9}_{-10}			$9.4^{+46}_{-42}\times10^{-3}$	$2.1^{+10}_{-10}\times10^{-3}$
		a	1251.6(12)	1497	17.5(9)	-0.03^{+19}_{-19}			$4.9^{+25}_{-23}\times10^{-3}$	$1.1^{+6}_{-5}\times10^{-3}$
		a	2005.5(15)	743	27.7(12)	-0.03^{+16}_{-16}			$1.9^{+10}_{-9}\times10^{-3}$	$1.6^{+8}_{-7}\times10^{-4}$
$5^{(-)}$	2750.34(21)	n	353.65(21)	2397	100	0.06^{+7}_{-6}				
	2762.0(2)	a,c	[357.2(4)]	2405						
		a	627.2(2)	2133						
1	2763.93(11)	n	1243.96(13)	1520	15.9(13)	*ind*	0.733(19)	24^{+3}_{-3}	$\leqslant$0.25	$\leqslant$59
		n	2020.73(17)	743	2.9(11)	*ind*			$\leqslant$0.014	$\leqslant$1.2
		n	2763.96(35)	0	81.2(17)				$9.1^{+16}_{-12}\times10^{-2}$	
	2776.95(12)	n	380.66(23)	2397						
		d,n	643.58(5)	2133						
1,(2)	2820.63(8)	a,e,m	852.15(11)	1969	19.4(17)	*ind*	0.224(21)	216^{+27}_{-24}	$\leqslant$0.11	$\leqslant$53
		n	1300.45(11)	1520	21.7(12)	*ind*			$\leqslant$0.031	$\leqslant$6.9
		a	2077.63(15)	743	51.8(20)	*ind*			$\leqslant$0.018	$\leqslant$1.6
		a	2821.39(40)	0	7.1(17)				$8.3^{+33}_{-27}\times10^{-4}$	
4^+	2830.66(10)	m,n	802.82(10)	2028	48.8(10)	0.03^{+104}_{-31}	0.127(35)	420^{+180}_{-110}	$1.3^{+5}_{-5}\times10^{-1}$	$6.6^{+29}_{-21}\times10^{-2}$
		n	2087.62(17)	743	51.2(10)					$6.5^{+24}_{-21}\times10^{-1}$
$5^{(-)}$	2851.87(29)	a	1040.40(26)	1811	68.0(25)	*E*1	0.324(109)	131^{+97}_{-48}	$1.8^{+11}_{-8}\times10^{-3}$W.u.	
		a	1354.85(53)	1497	32.0(25)	*E*1			$3.8^{+27}_{-18}\times10^{-4}$W.u.	
6	2861.91(21)	n	728.63(17)	2133	100	-1.04^{+28}_{-16}				
2^+,(1)	2869.15(12)	e,m,n	[675.8(5)]	2193			0.131(36)	410^{+180}_{-99}		
		n	890.24(26)	1979	9.6(13)					9.0^{+46}_{-37}
		n	900.48(13)	1968	9.7(13)	-0.44^{+35}_{-142}			$1.5^{+12}_{-15}\times10^{-2}$	1.6^{+37}_{-9}

TABLE I. *(Continued.)*

J^π	E_x (keV)	Note	E_γ (keV)	E_f (keV)	BR (%)	$\tan^{-1}(\delta)$	$F(\tau)$	τ (fs)	$B(M1)$ (μ_N^2)	$B(E2)$ (W.u.)
		a	1348.86(26)	1520	19.4(12)	0.06^{+186}_{-81}			$1.1^{+7}_{-5}\times10^{-2}$	$8.2^{+39}_{-40}\times10^{-3}$
		a	2125.67(28)	743	20.0(15)	-0.94^{+76}_{-78}			$1.0^{+17}_{-10}\times10^{-3}$	$1.6^{+80}_{-16}\times10^{-1}$
		a	2869.51(22)	0	41.3(16)					$1.1^{+5}_{-4}\times10^{-1}$
3	2884.42(14)	a,m	1364.45(51)	1520	16.2(12)	-0.69^{+44}_{-41}	0.099(7)	561^{+44}_{-44}	$3.8^{+20}_{-31}\times10^{-3}$	$5.3^{+51}_{-24}\times10^{-1}$
		a	2141.22(13)	743	83.8(12)	-1.19^{+19}_{-16}			$1.2^{+7}_{-11}\times10^{-3}$	$6.1^{+69}_{-31}\times10^{-1}$
5	2885.00(16)	n	1074.30(22)	1811	32.5(14)	-1.44^{+25}_{-22}	0.308(70)	141^{+57}_{-37}	$1.8^{+30}_{-14}\times10^{-3}$	34^{+43}_{-33}
		n	1387.76(16)	1497	67.5(14)	-0.13^{+10}_{-9}			$1.0^{+4}_{-4}\times10^{-1}$	$3.3^{+14}_{-11}\times10^{-1}$
2^+	2891.82(11)	a,c,m	1371.8(4)	1520	5.9(20)	*ind*	0.187(22)	270^{+42}_{-34}	$\leqslant7.4\times10^{-3}$	$\leqslant1.5$
		d,n	1394.45(34)	1497	5.0(32)					$7.5^{+66}_{-52}\times10^{-1}$
		a	2148.2(2)	743	24.4(20)	-0.94^{+60}_{-69}			$1.8^{+27}_{-17}\times10^{-3}$	$2.8^{+334}_{-28}\times10^{-1}$
		a	2891.98(14)	0	64.7(31)					$2.5^{+6}_{-5}\times10^{-1}$
4^+	2904.41(11)	m,n	876.62(12)	2028	46.4(13)	1.44^{+25}_{-25}	0.059(58)	970^{+690}_{-510}	$6.8^{+209}_{-35}\times10^{-4}$	19^{+27}_{-19}
		n	1384.46(25)	1520	41.4(13)					1.8^{+21}_{-8}
		n	2161.36(44)	743	12.2(12)					$5.7^{+74}_{-27}\times10^{-2}$
4^+	2912.79(12)	a,c	719.38(28)	2193	24.5(12)		0.036(24)	1630^{+3350}_{-670}		17^{+13}_{-12}
		d,g,n	1393.0(5)	1520	1.9(5)					$4.8^{+55}_{-36}\times10^{-2}$
		a	2169.57(13)	743	73.6(12)					$2.0^{+15}_{-14}\times10^{-1}$
0^+,(1–3)	2921.56(13)	c,e,m,n	1401.55(14)	1520	84.7(54)		0.035(65)	1700^{+3300}_{-1100}		2.0^{+44}_{-14}
		n	2178.5(24)	743	15.3(54)					$4.0^{+124}_{-31}\times10^{-2}$
	2931.86(10)	a,d	1434.85(6)	1497						
4,5,6	2953.02(29)	a	1141.5(17)	1811						
$3,4^+$	2954.83(7)	d,g,n	1434.85(6)	1520	67.6(10)		0.056(34)	1000^{+1700}_{-400}		
		n	2211.71(15)	743	32.5(10)	0.66^{+59}_{-19}				
5,6	2969.29(34)	d,g,n	1157.82(25)	1811						
3	2983.26(13)	a	1463.29(23)	1520	45.8(34)	-0.66^{+28}_{-31}	0.280(48)	160^{+45}_{-32}	$3.2^{+19}_{-20}\times10^{-2}$	3.4^{+29}_{-15}
		a	1486.24(14)	1497	34.8(31)	-0.72^{+63}_{-31}			$2.1^{+20}_{-14}\times10^{-2}$	2.8^{+27}_{-19}
		a	2240.09(73)	743	19.4(29)	-0.63^{+94}_{-100}			$4.0^{+40}_{-19}\times10^{-3}$	$1.6^{+11}_{-11}\times10^{-1}$
5	2986.30(18)	n	589.61(9)	2397	100	(*E*1)		510^{+1340}_{-230}	$3.7^{+31}_{-27}\times10^{-3}$W.u.	
1	2997.46(15)	n	1477.15(25)	1520	47.4(15)	0.94^{+100}_{-103}	0.299(37)	147^{+29}_{-31}	$2.0^{+30}_{-17}\times10^{-2}$	6.4^{+84}_{-63}
		n	2997.65(19)	0	52.6(15)				$7.5^{+23}_{-15}\times10^{-3}$	
6	2998.14(40)	n	1186.67(32)	1811	0.2(1)	-0.72^{+38}_{-145}				
2^+	3030.28(16)	e,n	836.2(5)	2193	9.3(28)		0.044(38)	1300^{+8700}_{-600}	$\leqslant0.018$	$\leqslant9.3$
		a	2287.06(15)	743	73.8(54)	-1.00^{+41}_{-41}			$7.7^{+157}_{-77}\times10^{-4}$	$1.3^{+90}_{-13}\times10^{-1}$
		a	3030.63(75)	0	16.9(52)					$1.1^{+17}_{-10}\times10^{-2}$
5(4)	3038.90(16)	n	467.71(23)	2572	52.7(13)	-0.72^{+28}_{-32}				
		n	905.37(15)	2133	47.3(13)	-0.60^{+19}_{-22}				
6^+(5,4)	3048.43(18)	d,n	1551.42(17)	1497	100					
4^+	3054.47(11)	n	1534.48(12)	1520	64.2(11)		0.134(6)	395^{+24}_{-18}		4.1^{+3}_{-4}
		n	2311.3(2)	743	35.8(11)					$2.9^{+3}_{-3}\times10^{-1}$
3	3067.17(9)	c,n,v	[1099.3(2)]	1968						
		n	873.24(20)	2193	16.0(10)	-0.09^{+18}_{-22}	0.134(6)	395^{+24}_{-17}	$3.4^{+5}_{-4}\times10^{-2}$	$1.4^{+2}_{-2}\times10^{-1}$
		a	1546.96(18)	1520	24.9(11)	0.09^{+16}_{-15}			$9.6^{+10}_{-10}\times10^{-3}$	$1.2^{+2}_{-2}\times10^{-2}$
		n	1570.61(18)	1497	27.2(10)	-0.38^{+32}_{-100}			$8.7^{+9}_{-2}\times10^{-3}$	$2.1^{+3}_{-3}\times10^{-1}$
		a	2323.87(19)	743	32.0(10)	0.31^{+29}_{-21}			$3.3^{+5}_{-7}\times10^{-3}$	$2.4^{+5}_{-4}\times10^{-2}$
4^+,(3)	3071.57(12)	d,g,n	1551.42(20)	1520	2.5(1)		0.249(48)	188^{+58}_{-40}		$3.2^{+11}_{-9}\times10^{-1}$
		n	1574.63(15)	1497	61.9(16)	-1.22^{+32}_{-34}			$5.7^{+64}_{-1787}\times10^{-3}$	6.4^{+3363}_{-48}
		n	2328.5(3)	743	35.6(15)					$5.9^{+20}_{-16}\times10^{-1}$

TABLE I. *(Continued.)*

J^π	E_x (keV)	Note	E_γ (keV)	E_f (keV)	BR (%)	$\tan^{-1}(\delta)$	$F(\tau)$	τ (fs)	$B(M1)$ (μ_N^2)	$B(E2)$ (W.u.)
6	3091.12(29)	n	957.84(26)	2133	100					
5,6	3097.63(27)	m,n	1600.61(26)	1497						
3,2	3100.55(16)	c,a	1580.56(18)	1520	51.9(16)	-1.35^{+19}_{-16}	0.279(47)	169^{+48}_{-34}		
		a	2357.43(27)	743	48.2(16)	0.91^{+31}_{-35}				
4^+	3101.40(13)	m,n	908.03(13)	2193	84(3)		0.172(77)	300^{+290}_{-110}		98^{+63}_{-50}
		n	1132.63(11)	1969	16(3)					6.2^{+6}_{-4}
1	3105.20(04)	a	3105.20(04)	0	100		0.276(35)	163^{+32}_{-24}	$1.2^{+2}_{-2}\times10^{-2}$	
4^+	3135.37(20)	n	1638.77(23)	1497	69.8(22)	0.41^{+38}_{-38}	0.149(82)	350^{+500}_{-150}	$2.1^{+23}_{-16}\times10^{-2}$	$5.7^{+70}_{-39}\times10^{-1}$
		n	2391.26(36)	743	30.2(22)					$2.3^{+20}_{-15}\times10^{-1}$
2^+	3137.98(29)	n	1617.88(39)	1520	33.4(15)	-0.97^{+97}_{-94}	0.263(40)	175^{+42}_{-31}	$8.2^{+114}_{-76}\times10^{-3}$	2.5^{+33}_{-25}
		a	2394.85(55)	743	11.2(9)	*ind*			$\leqslant3.5\times10^{-3}$	$\leqslant0.23$
		a	3138.23(61)	0	55.4(16)					$2.2^{+6}_{-5}\times10^{-1}$
3	3139.90(18)	m,n	645.81(34)	2494	33.3(20)	0.53^{+72}_{-84}				
		m,n	946.11(46)	2193	22.7(18)	0.03^{+44}_{-50}				
		m,n	1171.2(26)	1969	36.4(19)	-0.97^{+100}_{-35}				
		m,n	2397.3(55)	743	7.6(7)	0.41^{+148}_{-44}				
(6)	3146.40(91)	m,n	1118.63(90)	2028	100					
4^+	3148.31(11)	m,n	1628.25(11)	1520	76.0(9)		0.142(40)	370^{+170}_{-90}		
		n	2405.37(19)	743	24.0(9)					
	3150.80(20)	n	2407.60(19)	743						
(5)	3166.50(18)	m,n	1033.38(26)	2133						
		m,n	1138.63(22)	2028						
1	3185.61(53)	u,n	[2441.5(8)]	0	10(2)	(*E*1)	0.467(39)	73^{+12}_{-11}	$4.0^{+2}_{-1}\times10^{-5}$W.u.	
		a	3185.61(53)	0	90(2)	(*E*1)			$1.5^{+3}_{-2}\times10^{-4}$W.u.	
(5)	3188.20(35)	m,n	1691.19(34)	1497	100	1.29^{+16}_{-16}	0.290(131)	150^{+170}_{-66}		
3	3188.22(37)	m,n	2445.02(37)	743	100	-1.04^{+101}_{-31}	0.297(94)	148^{+95}_{-50}		
	3195.7(11)	d,n	1698.6(11)	1497						
	3199.2(17)	d,n	1702.1(17)	1497						
3	3217.22(22)	m,n	820.57(20)	2397	61(2)	0.81^{+54}_{-43}	0.371(157)	110^{+120}_{-50}		
		d,m,n	1697.15(45)	1520	39(2)					
	3219.4(4)	n	2476.1(4)	743						
	3221.48(3)	d,n	1701.2(13)	1520						
		n	1724.4(3)	1497						
	3249.4(4)	a	1729.4(4)	1520						
	3251.3(4)	n	1731.0(4)	1520						
	3255.0(4)	n	1735.0(4)	1520						
	3286.3(4)	n	1766.3(4)	1520						
	3297.1(4)	n	1776.9(4)	1520						
	3303.8(4)	n	1783.8(4)	1520						

[a] Adopted transition.
[c] See individual level discussion for this level.
[d] Doublet
[e] Branching ratios from excitation functions.
[g] Doublet intensities split using coincidence yields.
[k] Calculations show strength is probably missing from this level.
[m] Branching ratios not consistent with CINDY calculations.
[n] New transition.
[r] Reference [44].
[t] Triplet.
[u] Summed angle data.
[v] Assignment based on coincidence data only.

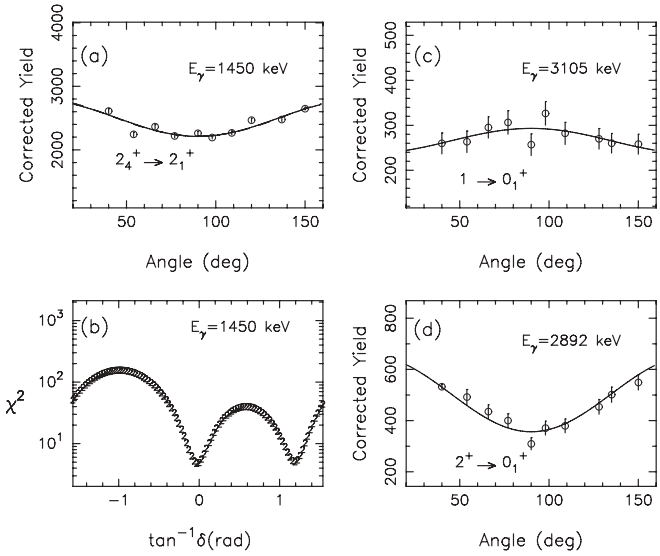

FIG. 3. Angular distribution, along with a Legendre polynomial fit to the data, for the 1450.2-keV γ ray from the 2193.5-keV level to the 2_1^+ level is shown in panel (a). In panel (b), the χ^2 vs $\tan^{-1}\delta$ curve used to obtain the multipole-mixing ratio for the transition in panel (a) is shown. Two solutions for the multipole-mixing ratio for spin $J = 2$ are suggested. γ-ray angular distributions for ground-state transitions from the 3105.2-keV ($J = 1$) and the 2891.5-keV ($J^\pi = 2^+$) levels are shown in panels (c) and (d), respectively.

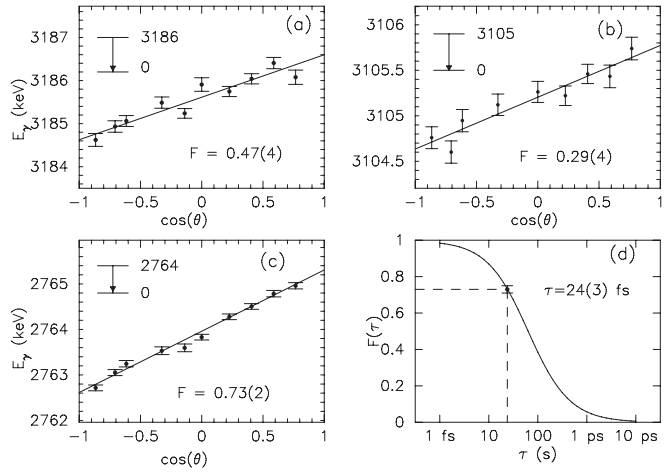

FIG. 4. Doppler shifts for the (a) 3186.6-keV, (b) 3105.2-keV, and (c) 2764.0-keV γ rays in ^{128}Te. Panel (d) shows the stopping theory calculations used to deduce τ from the Doppler shift of the 2764.0-keV γ ray shown in panel (c).

Figure 3(c) is an example of the χ^2 versus $\tan^{-1}(\delta)$ used to assess the spin and multipole-mixing ratio for the transition shown in Fig. 3(a). Often, two solutions for δ give similar values of χ^2; the value of δ with the smaller χ^2 is included in the table except where the state is discussed further in the paper, in which case both solutions are listed in Table I. Branching ratios were derived from the angular distribution data at the lowest incident neutron energy possible, unless otherwise noted.

Level lifetimes were extracted using the Doppler-shift attenuation method (DSAM) following inelastic neutron scattering [47]. Experimental lifetimes and unshifted γ-ray energies were found using the expression

$$E_\gamma(\theta) = E_o\left[1 + F(\tau)\frac{v_{\text{c.m.}}}{c}\cos(\theta)\right], \qquad (1)$$

where $E_\gamma(\theta)$ is the γ-ray energy as a function of laboratory angle θ, E_o is the unshifted γ-ray energy, $F(\tau)$ is the experimental Doppler-shift attenuation factor, $v_{\text{c.m.}}$ is the velocity of the recoiling nucleus in the center of mass, and c is the speed of light. Lifetimes were determined by comparing experimental and theoretical Doppler-shift attenuation factors, $F(\tau)$, calculated using the stopping theory of Winterbon [48]. Mean lifetimes in the range of a few fs to approximately 2 ps were determined in this experiment. The Doppler shifts for γ rays, as well as theoretical $F(\tau)$ calculations for the 2719-keV γ ray, are shown in Fig. 4.

Level energies, γ-ray placements, branching ratios, spin and parity assignments, multipole-mixing ratios, $F(\tau)$ values, lifetimes, and transition rates for all observed levels and transitions are given in Table I. New levels and transitions are noted by an "n" in the note column of Table I, while adopted levels and transitions [44] are indicated by an "a". Transition-rate uncertainties given in Table I include the statistical uncertainties in the level energies, the branching ratios, the multipole-mixing ratios, and the lifetimes. A systematic uncertainty of 10% is estimated for the lifetimes extrapolated using the Winterbon stopping theory [43]; however, this uncertainty is not included in the transition rate uncertainties in Table I. Systematic uncertainties from the energy calibration of $\Delta E = 0.2$ keV for $0 \leqslant E_\gamma \leqslant 500$ keV, $\Delta E = 0.05$ keV for $500 < E_\gamma \leqslant 2000$ keV, $\Delta E = 0.1$ keV for $2000 < E_\gamma \leqslant 3000$ keV, and $\Delta E = 0.5$ for $E_\gamma \geqslant 3000$ keV are included in the uncertainties of the γ-ray energies.

III. LEVEL DISCUSSION

Discrepancies between new information regarding levels and transitions in ^{128}Te and adopted values are explained in this section. Adopted levels [44] below 3.3 MeV not observed in this investigation include (1) high-spin states, typically not seen in $(n,n'\gamma)$ reactions, at 2689.4(5)(8^+), 2790.7(4)(10^+), and 3151.44(22)(6^+,7^+,8^+) keV; (2) states with large energy uncertainties, which may correspond to levels observed in this work, but the correspondence is not clear, that is, the 2440(20)-, 2520(10)-, 2720(50)-, 2790(10)-, 3000(10)-, 3160(20)-, and 3210(10)- keV states; and (3) the 1972(2)-, 2440(20)-, 2485(2)-, 2817.4(3)-, 2858.9(5)-, 2901.2(4)-, 2924.1(3)-, 3030.7(3)-, 3125.42(6)-, 3140.5(4)-, 3183.5(3)-, and 3210(10)-keV states, for which there is no obvious reason why they are not observed, other than that their excitation cross section is insufficiently large for the detection threshold of these new measurements, or these levels may have spins of $J > 6$. States that merit special attention are discussed in detail below.

1968.5-keV 2^+, (3^+) level. A 448.8-keV γ ray adopted [44] from this level is seen only in our summed angle data and in the 776-keV coincidence gate. An upper limit of 0.9%

can be assigned to this branch with the yield obtained from the summed spectra. The adopted spin and parity for this level is $J^\pi = 1^+, 2^+, 3^+$ [44]. The level is assigned $J^\pi = 2^+$ from reactor $(n, n'\gamma)$ measurements [30]. The $J = 2$ spin assignment consistently represents these new data, but the $J = 3$ assignment cannot be rejected.

2133.3-keV 5⁻ level. This level is adopted with decay γ rays of 322.3 and 636.3 keV [44]. The latter placement is confirmed in this work, while the former is an observed γ ray from a new level at 2457.7 keV that is observed in coincidence with the 636.3-keV γ ray. Excitation functions for the 323.5- and 636.3-keV transitions that show the different thresholds for these two γ rays are presented in Fig. 2.

2217.9-keV 1⁽⁺⁾ level. This level has an adopted spin and parity of $J^\pi = 1, 2^+$ and an adopted deexciting 249.2-keV γ ray [44]. Comparisons of the excitation functions for transitions from this level with CINDY calculations support the $J = 1$ spin assignment, although both $J = 1, 2$ are allowed from the angular distributions. The tentative positive-parity assignment comes from the systematics of the lowest 1^+ levels across the Te isotopic chain. The excitation function of the 249-keV γ ray observed in this work has a higher threshold and is observed in the 314-keV coincidence gate; it is assigned as deexciting the 2587.3-keV level.

2404.9-keV 4⁺,5,6⁺ level. This is an adopted level with 594- and 908-keV deexciting γ rays [44]. γ rays with these energies are seen in this work in the appropriate coincidence gates, but the 594-keV γ ray is in a region containing several background lines, and a much stronger 908-keV γ ray is associated with a level placed at 3101 keV in this work. The excitation function for the 908-keV γ ray exhibits no yield below 3 MeV, which indicates that the role of this γ ray in the deexcitation of a level at 2404.9 keV must be very small. Both transitions are labeled as tentative in Table I.

2487.4-keV 4⁺ level. This level is adopted with $J^\pi = 2^+, 3^+$ [44]. The angular distributions and excitation functions of the deexciting γ rays of 967.4, 990.4, and 1744.3 keV from these new measurements support $J^\pi = 4^+$.

2494.2-keV 3⁻ level. This level is adopted with $J^\pi = (3)^-$ [44]; the new data for the deexciting γ rays confirm the $J = 3$ spin assignment. Additional $J^\pi = 3^-$ states are adopted at 2440 and 2485 keV, but they are not observed in our measurements and must be spurious, thus making this the lowest 3^- state in ^{128}Te. A new 974.2-keV γ ray is assigned to this level from both excitation function and coincidence data; a 526.3-keV doublet γ ray is tentatively assigned from coincidence data and summed angle data only. The stronger component of the 526-keV γ rays is assigned to the 2338.5-keV level. The contributions of the 526-keV γ rays were split between the two levels by using integrations obtained from the summed angle data at 3.3 MeV.

2571.7-keV 5⁻ level. This level is adopted with 175.3-, 437.9-, and 1074.1-keV deexciting γ rays [44]. A 1074.3-keV γ ray is observed in this work with a higher threshold and is assigned to the 2885.0-keV level. Additionally, a new 760.2-keV γ ray is assigned to this level.

2599.2-keV 5⁺, 6⁺ level. This is an adopted level with deexciting γ rays of 193.5, 787.9, and 1101.8 keV [44]. A 787.5-keV γ ray is seen in all of the coincidence gates consistent with this placement, but nothing further can be determined because of the doublet nature of the peak. The 193.5-keV γ ray is not observed and a weak 1101.1-keV γ ray is observed but cannot be placed as deexciting this level, as it is not observed in the 753-keV coincidence gate.

2630.3-keV 3⁺ level. γ rays of 1132.9 and 1886.9 keV deexciting this level are adopted [44]. The 1887.1-keV γ ray is observed in this work and is assigned to this level; however, the 1132.6-keV γ ray observed in these new data has a higher threshold and is assigned as deexciting the 3101.4-keV level.

2655.4-keV level. This level is adopted with deexciting transitions of 249.7 (tentative), 844.0, and 1158.2 keV [44]. The 249-keV γ ray is assigned, deexciting a different level in this work. γ rays of 843.9 and 1158.3 keV are observed in the appropriate gates to be assigned as deexciting this state, but background and poor statistics prohibit any further details from being determined, and only a tentative assignment is made. The 1158.2-keV γ ray is also observed in the 314-keV gate which indicates that it is a doublet.

2706.8-keV 1 level. An 1186.7-keV γ ray is adopted as deexciting this level [44]. A peak with similar energy is observed with a higher threshold and is attributed to the decay of the 2998.1-keV level in this work. The angular distribution of the transition to the ground state unambiguously limits the spin of this level to $J = 1$.

2712.4-keV 1,(2,3) level. Observed γ rays of 1192.6 and 1969.0 keV agree with the adopted transitions deexciting this level [44]. The adopted transition to the ground state, however, is not observed in this work, even in the summed angle data. Branching ratios are listed for the two strong γ rays only; these are in good agreement with the relative intensities of the adopted values [44]. The preferred level spin is $J = 1$, provided that these two transitions account for almost all of the excitation strength.

2762.0-keV 4⁻,5⁻6⁻ level. Two γ rays are adopted deexciting this level [44]. Only the 357.2-keV transition is observed in the summed angle data, and it can only tentatively be placed as deexciting this level.

2912.8-keV 4⁺ level. A new γ ray of 1393.0 keV was assigned as deexciting this level based on the observation of the transition in the 776-keV coincidence gate. The angular distribution of the 2169.6-keV deexciting transition limits the spin of this level to $J = 3, 4$. Comparisons of the γ-ray production cross sections with statistical model calculations indicate that $J = 4$ is the preferred spin. Because all decays are to states with $J^\pi = 2^+$, the positive-parity assignment follows from the assumption that $M2$ decays are rarely observed.

2921.6-keV 0⁺,(1-3) level. The isotropic γ-ray angular distributions observed for γ rays from this level support the $J = 0$ spin assignment. Comparisons of γ-ray excitation function data with statistical model calculations also indicate a preference for the $J = 0$ assignment, although it is clear that there is missing decay strength. The transitions, however, are both weak with large uncertainties, making it impossible to exclude definitively the $J = 1, 2, 3$ spin assignments.

3067.1-keV 3 level. The 1547.0- and 2323.9-keV γ rays are adopted as deexciting this level [44], and three new deexciting transitions are reported here. The 1099.3-keV γ-ray placement is based on a strong peak in the 1225-keV $\gamma\gamma$

coincidence spectrum and is labeled as tentative because the excitation function and the angular distribution data exhibit a strong background contribution at this energy. The 873.2- and 1570.6-keV γ rays are also new assignments of deexciting transitions.

3139.9-keV 3 level. This new level is observed to decay by four deexciting transitions. The 645.8-keV γ ray is tentative because it cannot be verified in the $\gamma\gamma$ coincidence data unambiguously. This is a result of isotopic contaminants in the sample.

IV. MODEL CALCULATIONS

A. Overview

The excited levels of ^{128}Te exhibit several features characteristic of vibrational nuclei. For example, the ratio $E(4_1^+)/E(2_1^+)$ of 2.01 for ^{128}Te is almost exactly the harmonic value [44], and the energy and decay characteristics of the lowest 2_1^+ and 3_1^- states in ^{128}Te are typical of quadrupole and octupole phonons, respectively [2]. Levels exhibiting one-phonon MS character have also been observed in ^{128}Te [33].

Other excitations, such as intruder states from proton excitations across the $Z = 50$ closed shell, occur in many nuclei near $Z = 50$ [49–53], and specifically in the Te isotopes ^{120,122}Te [20,29,32,54], although they have not been clearly seen in $^{126–130}$Te, where such configurations are predicted to lie higher in energy and be more difficult to identify [19], as was found in ^{126}Te [29].

In $^{114–130}$Te, the 2_2^+ and 4_1^+ levels have previously been characterized as two-phonon excitations, while the 0^+ member of the triplet is identified as the 0_3^+ state in $^{122,124,(126)}$Te and the 0_2^+ state in $^{(126),128,130}$Te [20]. The difference is attributed to the energies of the 4p-2h configurations in these nuclei. The 0_2^+ level energy is significantly higher than is expected for a two-phonon state, but Lopac [2], using a two-particle plus vibrational model, was able to describe the increased energy of this level from the two-phonon region without including intruder configurations.

The three-quadrupole phonon quintuplet should lie at about 2.2 MeV in ^{128}Te, and it has previously been assigned as the 0_3^+, 2_6^+, 3_1^+, 4_3^+, and 6_1^+ levels [20]; these multiphonon assignments were based on the behavior of the multipole-mixing ratios and other systematic behavior across the Te isotopic chain and on comparisons with excitations in the Cd nuclei. Additionally, the $2_{3,4,5}^+$ states are considered to be two-quasiparticle states $(2qp)$ in that analysis. Calculations using the QPM indicate the 2_2^+ state is a member of the quadrupole two-phonon triplet, the 2_3^+ level is the three-phonon state, and the 2_4^+ level is the lowest MS state in ^{128}Te [25].

The 4^+ $2qp$ state has been identified in ^{128}Te as the 4_2^+ level in Ref. [20] by considering the preferential decay of the 4_1^- level into this state. The energy of the 4_2^+ state is observed to change by only 135 keV as one goes from ^{122}Te to ^{130}Te. This small change is attributed to contributions of the $1g_{7/2}$ and $2d_{5/2}$ proton orbits in the wave function of the 4_2^+ state; the 6_1^+ level energy is nearly constant for the even-A $^{122–130}$Te isotopes, possibly for the same reasons [3,20].

Two-quasiparticle calculations by Lee *et al.* [21] indicate the 6_1^+ state across the Te chain should occur at about 1.9 MeV and is composed mainly of the $\pi^2(2d_{5/2}, 1g_{7/2})$ and $\pi^2(1g_{7/2})^2$ configurations. Investigations of the 6_1^+ state with a two-particle-coupled-to-phonon excitations model revealed this level has essentially no three-phonon excitation strength and has a structure dominated by the two-proton $\pi^2(1g_{7/2})^2$ configuration, with a significant amplitude of one phonon coupled to two protons [22].

Clearly, many questions remain regarding the low-lying level structure of ^{128}Te. Through the measurements reported here, many new electromagnetic transition rates are provided for comparison to model calculations. In the following sections we compare the structures and transitions observed in ^{128}Te with model calculations using the interacting boson model (IBM-1 and IBM-2), the analytic U(5) limit of the IBM-2, and the particle-core coupling model (PCM). Calculated IBM and PCM transition rates are presented in Table III, while the U(5) analytic values, which were used only as a guide in identifying states with two-phonon MS character, are given in Table VII. In both tables, experimental values are included for comparison.

B. IBM calculations

1. IBM-1: U(5) model calculations

The IBM-1, in which neutron and proton motion is indistinguishable, has recently been used to examine in detail systematics across the Te isotopic chain [34,35]. The excitation energies of the lowest positive-parity levels in the Te isotopes and a limited set of electromagnetic transition rates for these nuclei were investigated in each of these studies, as well as two-neutron separation energies in Ref. [34]. The model parameters obtained were mapped onto the IBM symmetry triangle in Ref. [34] to show that ^{128}Te was best described within the U(5) vibrational limit of the model. The same conclusion was obtained in Ref. [35] in their investigation of the $Z = 52$ and $Z = 54$ isotopes. In this report, we compare new experimental data with IBM-1 calculations using PHINT [55]; the reader is referred to Refs. [35,55] for details of the model Hamiltonian. Model parameters for $^{120–126}$Te are listed in Ref. [35] and are the same for all the Te isotopes considered, except for the d-boson energy parameter (EPS). These same parameters are used in our calculations for ^{128}Te with EPS adjusted to reproduce $E(2_1^+)$. Level energies calculated using these parameters are shown in Fig. 5 and the parameters used are given in Table II. The experimental levels in Fig. 5 are separated into bands based only on their energies and not on any underlying structure for viewing purposes. All the observed positive-parity levels below 2.49 MeV are shown, except for the 1^+ level at 2.217 MeV, which is discussed later in the text; the 8_1^+ level energy was taken from Ref. [44] because such high spins are not typically observed in $(n,n'\gamma)$ measurements. The $E2$ transition operator used to calculate $B(E2)$ values is described in Refs. [35,55], and model parameters for ^{128}Te are given in Table II. Comparisons between experimental and calculated $B(E2)$ values are given in Table III.

TABLE II. Model parameters used in U(5) IBM-1 calculations [35].

N	EPS	ELL	QQ	CHQ	OCT	HEX	E2SD	E2DD
4	0.8620	−0.0059	−0.0300	−1.100	−0.0011	−0.0078	0.29	0

The model does not describe well the energy of the 0_2^+ level, which is observed experimentally over 300 keV higher in energy than the 2_2^+ and 4_1^+ levels. In Ref. [34], reproducing the energy of the 0_2^+ level in the Te nuclei required the addition of a term with $(d^\dagger\tilde{d})^{(4)}$. Adjustment of the strength of that term is controlled by the parameter HEX in our calculations. Increasing the strength of HEX did raise the energy of the 0_2^+ level in ^{128}Te, but the overall agreement, especially with higher-lying levels, did not improve. The calculated $B(E2; 0_2^+ \rightarrow 2_1^+)$ value is larger than the experimental value, indicating that the level is not as collective as the model predicts or that the experimental 0_2^+ level is not the best two-phonon candidate. The observed $B(E2; 0_3^+ \rightarrow 2_1^+)$ value, however, is also significantly smaller than the IBM-1 predictions and may indicate that intruder and few-particle configurations prohibit a clear identification of the 0^+ member of the two-phonon triplet. The model does do an excellent job describing the $B(E2)$ values for decays from the 2_2^+ and 3_1^+ states, as well as their energies, which supports these levels as members of the two- and three-phonon multiplets, respectively, in agreement with Ref. [20]. The energy of the 4_1^+ level is well represented by the model, but its lifetime has not been measured so its structure cannot be further assessed. The structure of the first six 2^+ levels has previously been discussed in Ref. [33]. In that reference, the 2_4^+ level was determined to be the lowest MS state in ^{128}Te with some admixture of MS strength into the 2_3^+ level. Comparisons between calculated and experimental $B(E2)$ values for $2^+_{(3-6)}$ levels in Table III show that none of these 2^+ levels can be unambiguoulsy identified as a three-phonon state. The decays of both the 4_2^+ and 4_3^+ levels into the 4_1^+ state agree with the IBM-1 calculations, but the observed decays into the 2_1^+ level do not agree. The experimental $B(E2; 6_1^+ \rightarrow 4_1^+)$ value is smaller than predicted for the three-phonon 6^+ state. This indicates that the level is not as collective as the model predicts and that single-particle configurations may play an important role in the structure of this level, in agreement with previous reports [3,20,21]. The experimental 6_2^+ level is only tentatively identified and no lifetime was determined, which prevents further assessment of its structure. In summary, for the IBM-1, the model does allow an unambiguous identification of some levels as two- and three- phonon states, but some observed states appear more complex than can be explained by the model. Further, the model does not predict as many low-lying positive-parity levels as are observed experimentally.

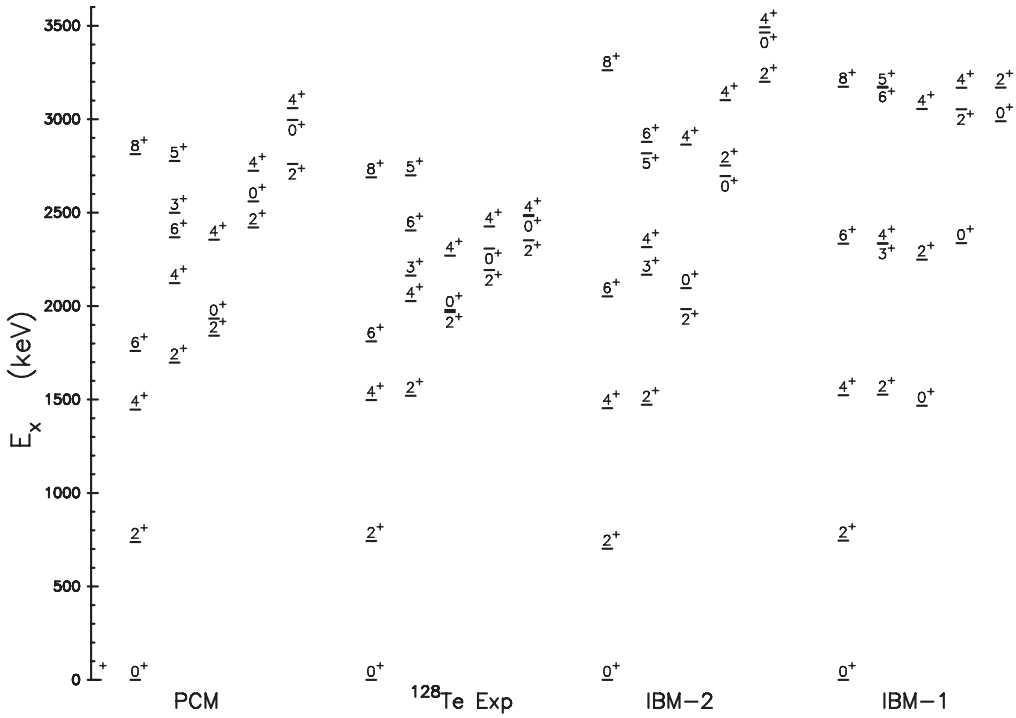

FIG. 5. Positive-parity levels in ^{128}Te compared to PCM, IBM-1, and IBM-2 calculated levels. The PCM calculations are new, while the IBM-1 and IBM-2 calculations were originally reported in Refs. [19] and [35], respectively. The levels are separated into quasibands based only on their order of appearance in energy.

TABLE III. Comparison of experimental transition rates for low-lying levels in ^{128}Te with IBM-1, IBM-2, and PCM calculations. $B(E2)$ values are in W.u. and $B(M1)$ values are in μ_N^2. Horizontal lines divide one-, two-, and three-phonon states in a vibrational picture. Below the double horizontal line are values for the $2^+_{4,5,6}$ states, because it is not obvious which experimental level corresponds to the 2^+_3 state of the IBM-2 calculations.

$B(\sigma\lambda; J_i^\pi \to J_f^\pi)$ (Theory)	J_i^π (Exp.)	J_f^π (Exp.)	B(XL) (Exp.)	IBM-1	IBM-2	PCM
$B(E2; 2_1^+ \to 0_1^+)$	2_1^+	0_1^+	[19.7(4)][a]	19.7	21.3	18.8
$B(E2; 4_1^+ \to 2_1^+)$	4_1^+	2_1^+		28.3	24.5	24.9
$B(E2; 2_2^+ \to 2_1^+)$	2_2^+	2_1^+	28(10)	28.1	19.2	28.5
$B(M1; 2_2^+ \to 2_1^+)$	2_2^+	2_1^+	0.0046^{+18}_{-9}		0.056	0.0012
$B(E2; 2_2^+ \to 0_1^+)$	2_2^+	0_1^+	0.034^{+13}_{-12}	0.047	0.026	0.033
$B(E2; 0_2^+ \to 2_1^+)$	0_2^+	2_1^+	3.6(17)	22.7	9.5	20.5
$B(E2; 0_3^+ \to 2_1^+)$	0_3^+	2_1^+	<1.0	0.031	0.0	0.096
$B(E2; 0_3^+ \to 2_2^+)$	0_3^+	2_2^+	<13	27.0	12.3	10.6
$B(E2; 2_3^+ \to 0_1^+)$	2_3^+	0_1^+		0.00	0.13	0.20
$B(E2; 2_3^+ \to 2_1^+)$	2_3^+	2_1^+	0.43^{+5}_{-4}	0.016	6.2	0.32
$B(M1; 2_3^+ \to 2_1^+)$	2_3^+	2_1^+	0.10^{+1}_{-1}		0.045	0.10
$B(E2; 2_3^+ \to 2_2^+)$	2_3^+	2_2^+	$\leqslant 35^{+41}_{-35}$	3.9	3.9	0.0079
$B(M1; 2_3^+ \to 2_2^+)$	2_3^+	2_2^+	$\leqslant 0.019^{+22}_{-19}$		0.016	0.011
$B(E2; 3_1^+ \to 2_1^+)$	3_1^+	2_1^+	0.25^{+8}_{-7}	0.047	0.052	0.065
$B(M1; 3_1^+ \to 2_1^+)$	3_1^+	2_1^+	0.0071(19)		0.0055	0.0033
$B(E2; 3_1^+ \to 2_2^+)$	3_1^+	2_2^+	15^{+5}_{-4}	19.4	25.3	4.1
$B(M1; 3_1^+ \to 2_2^+)$	3_1^+	2_2^+	0.090^{+22}_{-27}		0.022	0.034
$B(E2; 3_1^+ \to 4_1^+)$	3_1^+	4_1^+	12^{+7}_{-4}	7.8	7.3	2.8
$B(M1; 3_1^+ \to 4_1^+)$	3_1^+	4_1^+	0.042^{+13}_{-12}		0.022	0.0092
$B(E2; 4_2^+ \to 2_1^+)$	4_2^+	2_1^+	4.6^{+17}_{-16}	0.026	1.6	7.0
$B(E2; 4_2^+ \to 4_1^+)$	4_2^+	4_1^+	14^{+6}_{-6}	12.8	10.7	0.24
$B(M1; 4_2^+ \to 4_1^+)$	4_2^+	4_1^+	0.42^{+16}_{-15}		0.032	0.25
$B(E2; 6_1^+ \to 4_1^+)$	6_1^+	4_1^+	$[9.8^{+7}_{-6}]$[1]	27.3	20.3	12.2
$B(E2; 2_3^+ \to 0_1^+)$	2_4^+	0_1^+	0.51^{+3}_{-2}	0.00	0.13	
$B(E2; 2_3^+ \to 2_1^+)$	2_4^+	2_1^+	0.038^{+2}_{-2}	0.016	6.2	
$B(M1; 2_3^+ \to 2_1^+)$	2_4^+	2_1^+	0.24^{+1}_{-1}		0.045	
$B(E2; 2_3^+ \to 2_2^+)$	2_4^+	2_2^+		3.9	3.9	
$B(M1; 2_3^+ \to 2_2^+)$	2_4^+	2_2^+			0.016	
$B(E2; 2_3^+ \to 0_1^+)$	2_5^+	0_1^+	0.20^{+2}_{-2}	0.0	0.13	
$B(E2; 2_3^+ \to 2_1^+)$	2_5^+	2_1^+	0.31^{+3}_{-10}	0.016	6.2	
$B(M1; 2_3^+ \to 2_1^+)$	2_5^+	2_1^+	0.058^{+20}_{-6}		0.045	
$B(E2; 2_3^+ \to 2_2^+)$	2_5^+	2_2^+		3.9	3.9	
$B(M1; 2_3^+ \to 2_2^+)$	2_5^+	2_2^+			0.016	
$B(E2; 2_3^+ \to 0_1^+)$	2_6^+	0_1^+	0.11^{+2}_{-2}	0.0	0.13	
$B(E2; 2_3^+ \to 2_1^+)$	2_6^+	2_1^+	0.49^{+20}_{-13}	0.016	6.2	
$B(M1; 2_3^+ \to 2_1^+)$	2_6^+	2_1^+	0.010^{+3}_{-4}		0.045	
$B(E2; 2_3^+ \to 2_2^+)$	2_6^+	2_2^+		3.9	3.9	
$B(M1; 2_3^+ \to 2_2^+)$	2_6^+	2_2^+			0.016	

[a]Reference [44].

2. *IBM-2: Normal and intruder model calculations*

A comprehensive study of the even-even Te nuclei was completed by Rikovska *et al.* [19] using the IBM-2 in which neutron and proton motion is distinguishable, both with and without intruder-state mixing. These calculations revealed highly mixed intruder excitations in $^{116-124}$Te with low excitation energies that had signatures identifiable in the experimental data; for example, in ^{122}Te, an emerging intruder band was observed [32]. For the heavier Te isotopes, however, mixing calculations did not better represent the experimental

TABLE IV. Model parameters used in IBM-2 calculations from Ref. [19], both with and without intruder-state mixing.

	ϵ (MeV)	κ (MeV)	χ_π	χ_ν	ξ_1	ξ_2	ξ_3	e_π (e)	e_ν (e)	$C_{0\nu}$ (MeV)	$C_{2\nu}$ (MeV)	$C_{4\nu}$ (MeV)	α (MeV)	β (MeV)	Δ (MeV)	e_3/e_1
Normal	0.940	−0.267	−1.00	0.375	0.12	0.06	0.12	0.152	0.112	0.26	0.10	−0.35	0.21	0.105	5.172	0.91
Intruder	0.600	−0.367	−1.20	0.375	0.12	0.06	0.12	0.152	0.112	0.26	0.10	−0.35	0.21	0.105	5.172	0.91

data available at that time. These IBM-2 calculations for ^{128}Te ($N_\pi = 1$, $N_\nu = 3$), both with and without intruder-state mixing, have been repeated using the Hamiltonian, model parameters, mixing procedure obtained from the text and figures of Refs. [19,56], and the code NPBOS [57]. Model parameters used in both sets of calculations are given in Table IV and labeled "Normal" and "Intruder," respectively.

Calculations with intruder-state mixing were not found to improve the agreement between model and new experimental energies for low-lying states, because the first IBM-2 state with a significant intruder configuration (≈90%) was the 0^+_3 level calculated to occur near 2.6 MeV. The high level density in this region prohibited a clear identification of experimental intruder levels, similar to that observed in ^{126}Te [31]. No decays were observed into either the 0^+_3 or 0^+_4 levels, which would be expected if these states are intruder bandheads [19]. The calculated 0^+_3 and 2^+_4 levels are lower in energy than for the IBM-1 calculations discussed above. These states both have large intruder configurations (>85%) in the IBM-2 with mixing calculations, although they are not significantly lower in energy than is shown.

Calculated energies using the normal IBM-2 parameter set are shown in Fig. 5, labeled as IBM-2, in comparison to experimental data. The level energies are plotted as emerging bands with experimental levels ordered simply in terms of their energies. The average deviation for the levels shown is about 360 keV with most of this deviation from the highest two bands where the calculated energies are considerably higher than the observed levels. This result is not surprising because many of these low-lying levels have previously been identified as composed mainly of $2qp$ configurations [3,20–22] and may be outside the IBM-2 model space. The IBM-2 calculations better describe the experimental energies of the three-phonon triplet as the 0^+_2 energy is lifted above the the 4^+_1 and 2^+_2 states. As was observed in ^{122}Te [32], the model does not lead to the correct staggering of the 3^+ and 4^+ levels in the quasi-γ band, but overall the agreement between model calculations and the experimental level energies is good through the lowest three bands, but the calculated energies are much too large for the highest two bands. This staggering of levels in the quasi-γ band is observed to some degree in $^{114-130}$Te, and has been attributed to interactions between normal collective excitations, intruder levels, and $2qp$ admixtures [16].

Electromagnetic transition rates were calculated using the effective charges listed in Table IV and g factors of $g_\pi = 0.700\mu_N$ and $g_\nu = 0.150\mu_N$ from Ref. [19]. Results from the IBM-2 calculations are given in Table III. The transitions are divided into one-, two-, and three-phonon states by horizontal lines. Because it is not clear which experimental state corresponds to the IBM-2 2^+_3 state, experimental transition rates for the $2^+_{4,5,6}$ levels are compared to IBM-2 calculations below the double horizontal line. The 2^+_4 state has previously been identified as the lowest MS state in ^{128}Te, with the 2^+_3 state sharing the MS strength [33]. These 2^+ levels are further discussed in the next section, where overlaps with the analytic U(5) values are considered. The decay of the 0^+_2 state into the 2^+_1 state is better described by the IBM-2 calculations than by the IBM-1 values, although both attribute too much collectivity to the state compared to the experimental $B(E2)$ value; the 0^+_3 decays are also well described by the IBM-2 calculations. The $B(E2; 2^+_2 \rightarrow 0^+_1)$ value is well represented by the IBM-2, although the model overpredicts the collectivity of the decays of the 2^+_2 level to the 2^+_1 state. The calculated $M1$ rates are, in general, not as collective as that observed experimentally; this result is discussed in detail in Ref. [33] for the decays of the 2^+ levels. The quadrupole moment of the 2^+_1 level from these calculations is $Q_{2^+_1} = -0.16$ e b, which is of the correct sign but larger than the adopted experimental value of $Q_{2^+_1} = -0.06(5)$ e b [44].

While an exhaustive new best parameter search was not performed, varying just a few parameters significantly improved the agreement between experiment and theory for the energies of low-lying levels. The d-boson energy was reduced from $\epsilon = 0.94$ MeV to $\epsilon = 0.90$ MeV and the quadrupole-quadropole interaction strength parameter was reduced from $\kappa = -0.267$ MeV to $\kappa = -0.167$ MeV. The Majorana parameters were then adjusted from $\xi_1 = \xi_3 = 0.12$ and $\xi_2 = 0.06$ to $\xi_1 = \xi_3 = 0.24$, and $\xi_2 = 0.12$ to raise the energies of MS levels to near their expected energy region; for example, the lowest 1^+_1 state is a MS state in the U(5) limit of the IBM-2 and is expected to occur above 2.7 MeV (see below). The calculated 1^+_1 energy is still lower than the expected energy of the $1^+_{1,\mathrm{MS}}$ state in ^{128}Te, but increasing the Majorana parameters further resulted in larger deviations for lower-energy levels. While this new parameter set decreased the average deviation between experimental and calculated energies for the levels in Fig. 5, there was not a significant change in electromagnetic transition rates.

3. *IBM-2 U(5): Two-phonon MS states and overlap integrals*

$B(M1)$ and $B(E2)$ values were calculated using the U(5) analytic expressions for decays from symmetric and MS quadrupole one-phonon excitations and for decays from members of the $2^+_1 \otimes 2^+_{1,\mathrm{MS}}$ two-phonon quintuplet. Analytic U(5) expressions from Ref. [58,59] for $B(E2; 2^+_1 \rightarrow 0^+_1)$, $B(E2; 2^+_{1,M} \rightarrow 0^+_1)$, $B(E2; 2^+_{1,M} \rightarrow 2^+_1)$, and $B(M1; 2^+_{1,M} \rightarrow 2^+_1)$ were used as the basis for determining transition probabilities for decays from higher-lying MS levels. While

^{128}Te is certainly not expected to be an ideal U(5) nucleus, the calculations were used as a guide in identifying levels with two-phonon MS characteristics and to get approximate experimental effective charges and g-factor differences. The observed $B(E2; 2_1^+ \rightarrow 0_1^+)$ and $B(E2; 2_{1,M}^+ \rightarrow 0_1^+)$ values were used to deduce experimental proton and neutron boson effective charges of $e_\pi = 0.176(14)$ e b and $e_\nu = 0.125(14)$ e b, respectively, which were then used in further U(5) analytic calculations for other transitions. The values derived from the experimental data differed by about 20% from the values used in the normal IBM-2 calculations discussed above. Comparisons of experimental $B(M1; 2_{1,\mathrm{MS}}^+ \rightarrow 2_1^+)$ values with the reference expression for the same transition resulted in $|g_\nu - g_\pi|$ from $0.95\mu_N$ to $1.13\mu_N$, depending on whether only the 2193.5-keV MS level, or both the 2193.5-keV and the 1968.5-keV MS state $M1$ rates were considered [33]. The bare proton and neutron g factors of $g_\pi = 1\mu_N$ and $g_\nu = 0$ are within this range and were used for the analytic calculations. For the analytic calculations, $\chi_\pi = -1.0$ and $\chi_\nu = 0.375$ from Ref. [19] were used. The analytic calculations for $B(E2)$ and $B(M1)$ values for the symmetric and MS one-phonon excitations, as well as for members of the $2_1^+ \otimes 2_{1,\mathrm{MS}}^+$ quintuplet, are given in Table VII for comparison with experimental values. The importance of these calculations in evaluating MS excitations is discussed in greater detail below.

Additionally, the overlap of the IBM-2 wave functions from the calculations discussed above with the analytic U(5) wave functions was examined for the lowest levels to see which IBM-2 states contained the MS strength and which states contained the one-, two-, and three-phonon normal collective strength within the model; these overlaps are given in Table V.

TABLE V. Overlap integrals between IBM-2 and harmonic U(5) states in ^{128}Te. Only one IBM-2 1^+ state appears below 3.3 MeV and its wave function has a 97% overlap with the U(5) 1_{MS}^+ state.

IBM-2 state	$0_{1,S}^+$	U(5) $0_{2,S}^+(d^2)$	State $0_{3,S}^+(d^3)$	$0_{1,\mathrm{MS}}^+(d^2)$	
0_1^+	−0.906	0.353	0.057	0.024	
0_2^+	−0.313	−0.889	−0.128	−0.046	
0_3^+	−0.184	0.021	−0.784	−0.018	
0_4^+	−0.204	−0.189	0.565	−0.370	
0_5^+	−0.066	−0.188	0.158	0.859	
IBM-2 state	$2_{1,S}^+$	$2_{1,\mathrm{MS}}^+(d^1)$	$2_{2,S}^+(d^2)$	$2_{2,\mathrm{MS}}^+(d^2)$	$2_{3,S}^+(d^3)$
2_1^+	0.931	0.127	−0.148	−0.081	0.245
2_2^+	−0.143	0.686	−0.660	−0.115	−0.167
2_3^+	0.088	0.610	0.694	−0.202	−0.207
2_4^+	0.181	0.079	0.033	0.761	−0.487
2_5^+	−0.114	0.259	0.100	0.410	0.687
IBM-2 state	$3_{1,\mathrm{MS}}^+(d^2)$	$3_{1,S}^+(d^3)$			
3_1^+	0.823	−0.530			
3_2^+	0.500	−0.775			
3_3^+	0.154	−0.133			
IBM-2 state	$4_{1,S}^+(d^2)$	$4_{2,S}^+(d^3)$			
4_1^+	−0.939	−0.077			
4_2^+	−0.093	−0.7207			
4_3^+	−0.209	0.568			
4_4^+	−0.182	−0.046			

The U(5) wave functions were calculated using NPBOS with $\kappa \approx 0$, $C_{0\nu} = C_{2\nu} = C_{4\nu} = 0$, and the procedure discussed in Ref. [60]. The overlaps indicate that the IBM-2 0_2^+ state contains most of the two-phonon strength and the 0_3^+ state most of the three-phonon strength. The IBM-2 describes well the decay of these levels, which supports these structural assignments to the experimental levels. The IBM-2 0_4^+ state appears to contain the MS strength and is discussed further below. The overlaps indicate the calculated lowest $2_{1,\mathrm{MS}}^+$ strength is divided mainly between the IBM-2 2_2^+ and 2_3^+ levels, while little is predicted in the 2_4^+ state; however, the experimental 2_4^+ level was previously inferred to have most of the low-lying quadrupole MS strength in this nucleus in Ref. [33]. The parameters also result in a large amount of the quadrupole two-phonon strength assigned to the 2_3^+ level and three-phonon strength assigned to the 2_4^+ level, which is not supported by the experimental $B(E2; 2_3^+ \rightarrow 2_1^+)$ and $B(E2; 2_4^+ \rightarrow 2_3^+)$ values. The experimental 2^+ level appears to be a good two-phonon vibrational state provided the mixing ratio with the lower χ^2 value for the transition into the 2_1^+ level best describes its decay. The fact that many decays between 2^+ levels have two multipole-mixing solutions with nearly identical χ^2 values complicates the assignment of specific model structures to the individual levels, as was discussed previously in Ref. [33]. The overlaps indicate that the 3_1^+ level contains a significant amplitude of the two-phonon MS strength and that the 3_2^+ state contains most of the three-phonon strength. The MS strength is discussed in more detail below, but the experimental 3_1^+ level appears to be described even by the IBM-1 model, which supports the assignment of this level as the three-phonon state. Because lifetimes for the 4^+ states are not all available, it is difficult to compare theory and experiment, but the overlaps indicate that the IBM-2 4_1^+ is predominantly the two-phonon state and the IBM-2 4_2^+ level the three-phonon state.

C. Particle-core coupling model (PCM)

The ^{128}Te nucleus has been investigated previously with several models that include both particle and collective degrees of freedom [2,21,22,61,62]. We examine ^{128}Te levels using the code PPCORE [26,61,63] in light of our new experimental information. The PCM Hamiltonian, model parameter definitions, and electromagnetic transition operators are described in detail in Ref. [63]. Parameters specific to our calculations for ^{128}Te are given in Table VI, and model energies for low-lying, positive-parity levels are shown on the left side of Fig. 5 in comparison to experimental values. Techniques used to determine the best parameter set are described in Ref. [32].

Parameters which affect the $B(E2)$ values are the stiffness parameter, C_2, and the effective charge, e_{eff}, of the valence nucleons. The value of C_2 was determined from β_2, $\hbar\omega_2$, and the expression for C_2 given in Ref. [63]. The adjustable parameters for $M1$ transitions in the PCM are g_l, g_s, and g_R, which are the orbital, spin, and core gyromagnetic ratios, respectively. The values of g_s and g_R were kept fixed at $\frac{1}{2}g_{s,\mathrm{free}}$ and $g_R = Z/A$. The use of $g_l = 1.0$ in the calculations resulted in $\sum B(M1) = 0.0048{\mu_N}^2$ for the lowest seven $M1$

TABLE VI. Model parameters used in PCM calculations. The orbital energies are from Ref. [64].

Orbital Energies (keV)					Pairing	Phonon Energies (keV)		Couplings		e_{eff}	Stiffness (MeV)		(MeV)
$g_{7/2}$	$d_{5/2}$	$h_{11/2}$	$d_{3/2}$	$s_{1/2}$	G	$\hbar\omega_2$	$\hbar\omega_3$	ξ_2	ξ_3	(e)	C_2	C_3	$\langle r\partial V/\partial r\rangle$
0	963	2760	2690	2990	0.23	1214	2343	1.71	1.15	1.05	358	571	40

transitions, which is significantly smaller than that observed experimentally, so a value of $g_l = 0.5$ was used for the calculations presented. Results for $B(E2)$ and $B(M1)$ values from PCM calculations, along with experimental values, are given in Table III.

The average deviation between the calculated and experimental energies for the levels shown in Fig. 5 is about 185 keV. The energies of the first three 2^+ levels are well described by the model. The $2^+_{1,2,5}$ states have PCM wave functions with large amplitude of one- and two-phonon coupled to two-particle configurations, while the $2^+_{3,4}$ states have wave functions strongly dominated by two-particle configurations. In fact, the energies are in very good agreement through the first three bands, with the exception of the order of the 3^+_1 and 6^+_2 levels. The PCM wave function for the 3^+_1 level is composed of about 12% $\pi^2(1g_{7/2}, 2d_{5/2})$, 50% $(1\hbar\omega_2 \otimes \pi^2 1g_{7/2})^2$, and about 9% is spread in various two-phonon configurations. The $\pi^2(1g_{7/2})^2$ and $\pi^2(1g_{7/2}, 2d_{5/2})$ configurations make up almost 70% of the PCM 6^+_2 level, which lies only 40 keV lower than the tentative 6^+_2 experimental level. The PCM predicts a collective $B(E2 : 3^+_1 \rightarrow 2^+_2)_{\text{PCM}} = 4.1$ W.u., but this value is smaller than the experimental value of 12^{+7}_{-4} W.u. The transition rates for the other decays of the 3^+_1 level are also larger than the model predicts, although they do not appear to be very enhanced. The $B(E2; 4^+_2 \rightarrow 4^+_1)$ value also seems to be significantly larger than the PCM predicts, although other calculated $B(E2)$ values for transitions from this level are in reasonably good agreement with the experimental values. For $M1$ transitions, reducing $g_l = 1$ to $g_l = 0.5$ better represents what is observed experimentally, although the small $B(M1)$ values obtained with $g_l = 1.0$ may simply indicate that the PCM does not adequately represent the magnetic features of these low-lying transitions. Overall, the PCM $B(E2)$ and $B(M1)$ values agree very well with the experimental values for most transitions listed in Table III, and the model appears to better represent the structure of ^{128}Te than does the IBM-2, at least with the IBM-2 parameter set used.

V. SPECIAL COLLECTIVE AND FEW-PARTICLE STRUCTURES

A. Mixed-symmetry states

1. One-phonon mixed-symmetry states

The experimental 2^+_4 state at 2193.5 keV was previously identified as the lowest MS state in ^{128}Te with possibly a component of the MS strength observed in the 1968.5-keV level [33]. Investigations of higher-lying excitations in ^{128}Te have revealed additional support for the 1968.5-keV level as sharing the MS strength in this nucleus. The observed 526.2-keV transition is newly identified as a decay from the 3^-_1 level to the 1968.5-keV level (see level discussion). The $3^-_1 \rightarrow 2^+_{1,\text{MS}}$ transition was observed in many nuclei near $N = 84$ and determined to be a good indicator of MS strength in 2^+ levels; furthermore, the $B(E1; 3^-_1 \rightarrow 2^+_{\text{MS}})$ was consistently found to be larger than $B(E1; 3^-_1 \rightarrow 2^+_{1,S})$ [65]. The 526.2-keV $3^-_1 \rightarrow 2^+_3$ decay has a $B(E1; 3^-_1 \rightarrow 2^+_3) = 2.4^{+6}_{-5} \times 10^{-4}$ W.u., which is slightly larger than the observed $B(E1; 3^-_1 \rightarrow 2^+_1) = 1.9^{+2}_{-2} \times 10^{-4}$ W.u. The absence of the $3^-_1 \rightarrow 2^+_{1,\text{MS}}$ for the 2193.5-keV level is not unusual for the Te isotopes, because searches for the $3^-_1 \rightarrow 2^+_{1,\text{MS}}$ transitions in $(n,n'\gamma)$ studies on ^{122,124,126}Te reveal no other transitions. What is consistently observed across the Te isotopes are $B(E1 : 3^-_1 \rightarrow 2^+_1)$ values on the order of 10^{-4} to 10^{-5} W.u. and that the 3^-_1 levels decay to the 2^+_1, 4^+_1, and 2^+_2 states. The $B(E1 : 3^-_1 \rightarrow 2^+_1)$ values observed for the Te nuclei are at least an order of magnitude smaller than that observed in ^{92}Zr, ^{94}Mo, and ^{142}Ce for the $3^-_1 \rightarrow 2^+_{1,\text{MS}}$ transition [65]. Both the 1968.5-keV and the 2193.5-keV levels are considered to have fragmented MS strength in the assessment of higher-lying MS levels discussed below.

2. Two-phonon mixed-symmetry states

The coupling of the lowest $2^+_{1,\text{MS}}$ state to the quadrupole phonon, the lowest $2^+_{1,S}$ level, is expected to lead to a quintuplet of levels $(2^+_{1,S} \otimes 2^+_{1,\text{MS}})_{(0-4)^+}$. Candidates for members of this two-phonon multiplet have been identified previously in other nuclei; for example, in ^{94}Mo the 1^+, 2^+, and 3^+ members of the multiplet have been observed [66,67] and in ^{96}Mo the two-phonon MS strength is observed to be fragmented [68]. The energy of this two-phonon multiplet is expected to be near the sum of $E(2^+_{1,S}) + E(2^+_{1,\text{MS}})$, which due to the fragmentation of the $2^+_{1,\text{MS}}$ strength is expected to be between about 2.7 to 3.0 MeV in ^{128}Te. Characteristics of the two-phonon MS states are discussed in detail in Ref. [69]. Identification of experimental levels most characteristic of this two-phonon multiplet is guided by decay properties: specifically, by observed decays into one or both of the the $2^+_{1,\text{MS}}$ levels, and by comparisons to reduced transition probabilies calculated using analytic expressions from the U(5) limit of the IBM-2 from Ref. [59], which are given in Table VII along with deduced experimental values. Candidates for the MS quintuplet in ^{128}Te are discussed below.

MS 0^+ level. The 2921.6-keV level is the only possible 0^+ level in the energy region of interest for the $0^+_{1,\text{MS}}$ state. This level is not observed to decay to either of the $2^+_{1,\text{MS}}$ states, and while the observed lifetime is large, a several-hundred-fs lifetime is attainable within a standard deviation. The overlaps

TABLE VII. Comparisons of experimental and analytical expressions for the reduced electromagnetic transition strengths in the U(5) limit of the IBM-2 for states of mixed neutron-proton symmetry. Analytical values are from Ref. [59]. The $2^+_{1,\mathrm{MS}}$ strength is fragmented in the 1968.5- and 2193.5-keV levels; this splitting of MS strength is also observed in some members of the $2^+_{1,\mathrm{MS}} \otimes 2^+_{1,\mathrm{MS}}$ quintuplet. Decays to these $2^+_{1,\mathrm{MS}}$ states are distinguished by ↓1969 and ↓2193, respectively, in the column "Level energy."

Q	Transition	$B(E2)$ U(5) (W.u.)	$B(M1)$ U(5) (μ_N^2)	Level energy (keV)	$B(E2)$ Exp. (W.u.)	$B(M1)$ Exp. (μ_N^2)	Level energy (keV)	$B(E2)$ Exp. (W.u.)	$B(M1)$ Exp. (μ_N^2)
$2^+_{1,S}$				743.2					
	$2^+_{1,S} \to 0^+_1$	19.8			19.7^{+4}_{-4}				
$2^+_{1,M}$				2193.5			1968.5		
	$2^+_{1,M} \to 0^+_1$	2.4			0.51^{+3}_{-2}				
	$2^+_{1,M} \to 2^+_1$	3.3	0.27		0.038^{+2}_{-2}	0.24^{+1}_{-1}		0.42^{+5}_{-4}	0.10^{+1}_{-1}
	$2^+_{1,M} \to 2^+_2$	0.40						<39	<0.02
	$2^+_{1,M} \to 4^+_1$	0.71							
	$2^+_{1,M} \to 0^+_2$	0.08							
$2^+_{1,S} \otimes 2^+_{1,M}$									
$0^+_{1,M}$				2921.6					
	$0^+_{1,M} \to 2^+_{1,S}$	1.2			0.04^{+124}_{-31}				
	$0^+_{1,M} \to 2^+_{2,S}$	4.5			2.0^{+44}_{-14}				
	$0^+_{1,M} \to 2^+_{3,S}$	2.8							
	$0^+_{1,M} \to 2^+_{1,M}$	3.6							
$1^+_{1,M}$				2763.9			2820.6		
	$1^+_{1,M} \to 0^+_{1,S}$		0			$9.1^{+16}_{-12} \times 10^{-4}$			$8.3^{+33}_{-27} \times 10^{-4}$
	O(6)		0.14						
	$1^+_{1,M} \to 2^+_{1,S}$	2.4			$\leqslant 1.2$	$\leqslant 0.014$		$\leqslant 1.6$	<0.018
	$1^+_{1,M} \to 2^+_{2,S}$	2.2	0.42		$\leqslant 59$	$\leqslant 0.25$		$\leqslant 6.9$	<0.031
	$1^+_{1,M} \to 0^+_{2,S}$		0.24						
	$1^+_{1,M} \to 2^+_{1,M}$	19.8					↓1969	$\leqslant 53$	$\leqslant 0.11$
	$1^+_{1,M} \to 3^+_{1,S}$	0							
	$1^+_{1,M} \to 2^+_{3,S}$	0							
$2^+_{2,M}$				2869.1			3030.3		
	$2^+_{2,M} \to 0^+_{1,S}$				0.11^{+5}_{-4}			$1.1^{+17}_{-10} \times 10^{-2}$	
	$2^+_{2,M} \to 2^+_{1,S}$	1.2			0.16^{+80}_{-16}	$1.0^{+17}_{-10} \times 10^{-3}$		$1.3^{+90}_{-13} \times 10^{-1}$	$7.7^{+157}_{-77} \times 10^{-4}$
	$2^+_{2,M} \to 2^+_{2,S}$	0.20	0.09		$8.2^{+39}_{-40} \times 10^{-3}$	0.011^{+7}_{-5}			
	$2^+_{2,M} \to 0^+_{2,S}$	0.89			9.0^{+46}_{-37}				
	$2^+_{2,M} \to 4^+_{1,S}$	0.65							
	$2^+_{2,M} \to 2^+_{3,S}$	0.23							
	$2^+_{2,M} \to 2^+_{1,M}$	3.6		↓1969	1.6^{+37}_{-9}	0.015^{+12}_{-15}	↓2193	$\leqslant 9.3$	$\leqslant 0.018$
$3^+_{1,M}$				2748.9			3067.2		
	$3^+_{1,M} \to 2^+_{1,S}$	2.4			$1.6^{+8}_{-7} \times 10^{-4}$	$1.9^{+10}_{-9} \times 10^{-3}$		0.024^{+5}_{-4}	$3.3^{+5}_{-7} \times 10^{-3}$
	$3^+_{1,M} \to 2^+_{2,S}$	2.9	0.20		$2.1^{+10}_{-10} \times 10^{-3}$	$9.4^{+46}_{-42} \times 10^{-3}$		0.012^{+2}_{-2}	$9.6^{+10}_{-10} \times 10^{-3}$
	$3^+_{1,M} \to 4^+_{1,S}$	4.1	0.15		$1.1^{+6}_{-5} \times 10^{-3}$	$4.9^{+25}_{-23} \times 10^{-3}$		0.21^{+3}_{-3}	$8.7^{+9}_{-2} \times 10^{-3}$
	$3^+_{1,M} \to 2^+_{1,M}$	19.8		↓2193	$\leqslant 17$	$\leqslant 0.018$	↓2193	0.14^{+2}_{-2}	0.034^{+5}_{-4}
	$3^+_{1,M} \to 2^+_{1,M}$	19.8		↓1969	1.1^{+7}_{-6}	0.022^{+12}_{-11}	↓1969		
	$3^+_{1,M} \to 2^+_{3,S}$	0							0
$4^+_{1,M}$				2912.8			3101.4		
	$4^+_{1,M} \to 2^+_{1,S}$	1.2			0.20^{+15}_{-14}				
	$4^+_{1,M} \to 4^+_{1,S}$	2.5	0.30		$1.6^{+8}_{-7} \times 10^{-4}$	$1.9^{+10}_{-9} \times 10^{-4}$			
	$4^+_{1,M} \to 2^+_{2,S}$	0.36			0.048^{+55}_{-36}				
	$4^+_{1,M} \to 2^+_{3,S}$	0.23							
	$4^+_{1,M} \to 2^+_{1,M}$	3.6		↓2193	17^{+13}_{-12}		↓2193	98^{+63}_{-50}	
	$4^+_{1,M} \to 2^+_{1,M}$	3.6					↓1969	6.2^{+6}_{-4}	

between U(5) analytic and IBM-2 wave functions for 0^+ levels given in Table V indicate that the IBM-2 0^+_4 state near 3.0 MeV contains about 85% of the two-phonon MS strength. The observed B($E2$) values for the decays of this level into the 2^+_1 and 2^+_2 states are in agreement with the expected decays of the $0^+_{1,\mathrm{MS}}$ state, as shown in Table VII; nonetheless, the

assignment of this state as the $0^+_{1,\mathrm{MS}}$ candidate is tentative, especially because the level is near the expected energy of the 0^+ member of the quadrupole four-phonon octet.

MS 1^+ level. Candidates have been identified for the 1^+_{MS} state in $^{122-126,130}$Te [24,25,27,28], but in ^{128}Te, the important transition rates between levels in the region where $2^+_{1,S} \otimes 2^+_{1,\mathrm{MS}}$ states are expected and specific low-lying MS and symmetric collective excitations have not been previously identified. Seven spin-1 states with lifetimes of a few hundred femtoseconds or less and undetermined parity are observed in the 2.5- to 3.3-MeV region; the levels with ground-state transitions are shown in panel (a) of Fig. 6, along with arrows indicating the expected energies of the QOC and MS states based on the sum of the appropriate one-phonon energies. Because the parities are unknown for these $J = 1$ states, identification of the best candidates for the 1^+ MS states is guided by expected MS decay characteristics, model calculations, and systematics across the Te isotopic chain, as well as across other nearby isotopic chains [25,70,71]. The $B(M1)$ values for assumed positive parity are shown for each of these $J = 1$ states in panel (b) of Fig. 6.

Quasiparticle-phonon model calculations [25] predict the $1^+_{1,\mathrm{MS}}$ state occurs at 2.963 MeV in ^{128}Te and decays to the ground state with a B($M1$) value shown in panel (b) of Fig. 6. The calculated QPM $M1$ rates have previously been found to be about 1.5–1.7 times larger than the experimentally observed values for the 1^+ states across the Te chain [25]. According to quasiparticle random-phase approximation

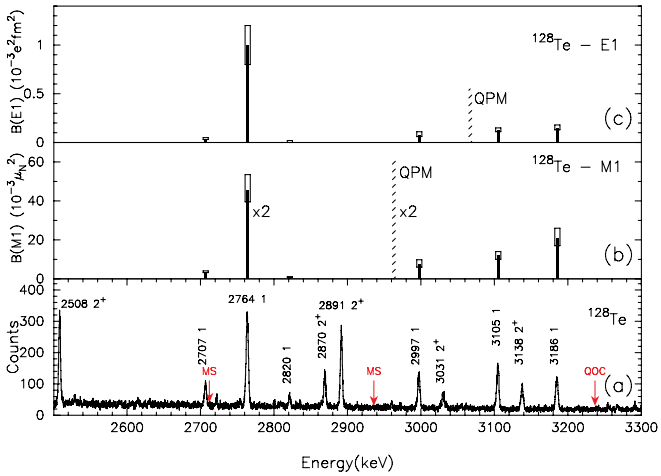

FIG. 6. (Color online) Panel (a) shows the summed-angle spectrum for ^{128}Te for γ-ray energies between 2.5 and 3.3 MeV with ground-state transitions labeled with the energy of the γ ray and the spin of the originating level, if known. The arrows labeled QOC and MS are at the summed energy of the 2^+_1 and 3^-_1 levels and the 2^+_1 and $2^+_{1,\mathrm{MS}}$ levels, respectively. The $M1$ and $E1$ reduced transition probabilities for ground-state decays from $J = 1$ levels identified below 3.3 MeV excitation in ^{128}Te are shown for assumed positive parities in panel (b) and for assumed negative parities in panel (c) to assess the MS and QOC characters of these states. The calculated QPM value [25] is also shown for each assumed parity. Uncertainties in $B(E1)$ and $B(M1)$ values are indicated by the boxes on the vertical bars.

(QRPA) calculations, the fragmentation of $2^+_{1,\mathrm{MS}}$ strength leads to fragmentation of MS strength in the $(2^+_{1,S} \otimes 2^+_{1,\mathrm{MS}})$ quintuplet and it is tentatively observed in dipole excitations in the even-even $^{122-126,130}$Te nuclei [28]. Within the U(5) limit of the IBM-2 model, $M1$ decays of the 1^+_{MS} state to either the ground state or the 2^+_1 level are forbidden because of phonon selection rules, but most nuclei are best described outside the model space of the dynamical symmetries [69].

The relative size of the branching ratios for the decays to the ground state and to the 2^+_1 level for each of the observed $J = 1$ states in the 2.5- to 3.3-MeV region indicates the 2706.7-, 2820.6-, and possibly the 2997.5-keV states are the most likely MS states, because previous studies of MS and QOC states in the Te nuclei indicate the QOC state is dominated by the decay to the ground state, while the MS state has a larger branch to the 2^+_1 level [25]. Only the 2820.6-keV level is observed to have a definite decay into the $2^+_{1,\mathrm{MS}}$ state at 1968.5 keV, and it is the best candidate for the 1^+_{MS} state based on decay characteristics and the level lifetime of 216^{+27}_{-24} fs. Only an upper limit for $B(M1)$ and $B(E2)$ values can be determined for most transitions from the 2820.6-keV level; these are shown in Table VII with comparison to U(5) values for decays from the $1^+_{1,\mathrm{MS}}$ state. The experimental $B(E2)$ values agree reasonably well with U(5) calculations, but the experimental $M1$ rates are much smaller than model values. The observed $B(M1; 1^+ \rightarrow 0^+_1)$ for the 2820.6-keV level is also well below the QPM value, but in a vibrational picture this two-phonon transition should be zero. Comparison of experimental $B(M1)$ values with the QPM value in Fig. 6 indicates that the 2763.9-keV level is the best MS candidate in ^{128}Te based on the observed $B(M1; 1^+ \rightarrow 0^+_1)$ value, provided this is a positive-parity state, because the level also has the best QOC state characteristics, as discussed below. A lower-lying 1^+ level exists at 2217.9 keV, but this level is well below the 1^+_{MS} state predicted near 3 MeV by IBM-2 calculations [19] or the energy expected from summing the 2^+_1 and $2^+_{1,\mathrm{MS}}$ level energies; this level is discussed in greater detail below. Clearly, questions will remain until the parities of these levels are determined.

MS 2^+ level. Levels at 2869.2 and 3030.3 keV are observed to decay into one or both of the $2^+_{1,\mathrm{MS}}$ levels. The 2869.2-keV level has a lifetime in the range characteristic of MS-state lifetimes. The level also decays to both of the low-lying $2^+_{1,\mathrm{MS}}$ states with transition rates which agree with some of the U(5) analytic values shown in Table VII; for example, the decay from this state into the 2^+_2 state is of the same order of magnitude as the U(5) $B(M1; 2^+_{2,\mathrm{MS}} \rightarrow 2^+_{2,S})$ value. The tentative identification of the 3030.3-keV level as sharing $2^+_{2,\mathrm{MS}}$ strength is based only on the observed decay into the 2193.5-keV level, because the observed $M1$ transition rates are small, the lifetime of the level is long, and the predicted decay to the 2^+_2 level is not observed.

MS 3^+ level. $J = 3$ levels at 2748.9 and 3067.1 keV exhibit decay characteristics consistent with the $3^+_{1,\mathrm{MS}}$ state. Each of these levels decays into one or both of the $2^+_{1,\mathrm{MS}}$ levels and undergoes decays consistent with those predicted in the U(5) limit of the IBM-2, as shown in Table VII. The observed transition rates, especially the $M1$ rates, do not

agree well with model predictions, and the lifetime of the 2748.9-keV level is larger than expected for a two-phonon MS state.

MS 4^+ level. The 4^+ level at 2912.8 keV exhibits decays consistent with a MS interpretation. Its decay into the 2193.5-keV level with a collective $B(E2; 4^+_{1,\mathrm{MS}} \rightarrow 2^+_{1,\mathrm{MS}}) = 17^{+13}_{-12}$ compares well with $B(E2; 2^+_1 \rightarrow 0^+) = 19.7(2)$ W.u. [44], as expected for MS states [69], although it is larger than U(5) predictions in Table VII. The two-phonon MS states should decay into the symmetric 2^+_1 level with a strength comparable to that of the $B(E2 : 2^+_{1,\mathrm{MS}} \rightarrow 0^+_1) = 0.51(2)$ W.u., which compares well with the observed value of $B(E2; 4^+_{1,\mathrm{MS}} \rightarrow 2^+_1) = 0.20^{+15}_{-14}$ W.u. While these decays strongly support this level as a two-phonon MS state, the mean lifetime of $1.6^{+3.4}_{-0.7}$ ps is longer than the few hundred fs expected for MS levels in vibrational nuclei [69]; additionally, the expected $4^+_{1,\mathrm{MS}} \rightarrow 4^+_{1,S}$ $M1$ transition is much weaker than U(5) predictions. There are several other 4^+ levels in the appropriate energy region, many with faster lifetimes, but none of them are observed to decay into either of the $2^+_{1,\mathrm{MS}}$ states, except for the 3101.5-keV level, which is observed to decay into both the 1968.5- and the 2193.5-keV levels with collective $E2$ transitions. Although no other MS characteristic decays are observed for this level, the 4^+ MS strength may be split between it and the 2912.8-keV level.

In summary, MS states are best identified by large $M1$ decay rates to specific levels; however, $B(M1; 2^+_{1,\mathrm{MS}} \rightarrow 2^+_{1,S})$'s are only $0.24(1)\mu^2_N$ and $0.10(1)\mu^2_N$ for the 2193.5- and 1968.5-keV levels, respectively, and this strength is expected to be fragmented in the higher-lying levels just as for the $2^+_{1,\mathrm{MS}}$ states [28]. While there is some evidence of two-phonon MS strength in the levels discussed above, there remain ambiguities in each case. Missing parity information for most of these levels limits the analysis.

B. Quadrupole-octupole coupled multiphonon states

Coupling between quadrupole and octupole vibrational modes, or QOC states, should produce a quintuplet of levels with spins 1^-, 2^-, 3^-, 4^-, and 5^-. In a simple phonon model, these states are predicted to lie at an energy given by the sum of $E(2^+_1)$ and $E(3^-_1)$, which is $\simeq$3237 keV in ^{128}Te. Ideally, $E3$ transitions from this quintuplet of QOC states to the 2^+_1 and $E2$ transitions into the 3^-_1 should have $B(E3)$ and $B(E2)$ values of the same strength as $B(E3; 3^-_1 \rightarrow 0^+_1)$ and $B(E2; 2^+_1 \rightarrow 0^+_1)$, respectively [37]. In practice, one usually cannot observe large $E3$ strength into the quadrupole phonon, as the faster $E1$ decays dominate. Candidates for these states have been identified in other nuclei in this mass region. For example, ^{122}Te, [27,32], ^{124}Te [23], and ^{122,124,126,130}Te [25,28] have all had at least the 1^- QOC candidates observed, but in ^{128}Te these states have not been previously identified. The candidates for QOC states in ^{128}Te are guided by experimentally deduced $B(E1)$ and $B(E2)$ values, observed decay branches, QPM calculations [25], and *spdf* IBM-2 calculations [69].

QOC 1^- state. The 1^-_{QOC} state is often observed within 250 keV or so of the sum of $E(2^+_1)$ and $E(3^-_1)$. Panel (a) of Fig. 6 shows transitions from $J = 1$ states in ^{128}Te in the region where the QOC state is expected to occur and $E1$ rates for assumed negative parity for each of these states is shown in panel (c) along with the QPM predicted energy and $B(E1)$ value. Candidates for the QOC 1^- state are guided by comparisons with model calculations and behaviors observed in the other Te nuclei. In ^{122}Te [32], ^{124}Te (unpublished), and ^{126}Te the QOC 1^- candidates have lifetimes of 26(2), 42(3), and 39^{+4}_{-3} fs, respectively, and in both ^{122}Te and ^{124}Te exhibit strong (>65%) decay branches to the ground state and about 20% branches to the 2^+_1 state, while for ^{126}Te only a ground-state decay of the 2974.6-keV level is reported [31].

For $J = 1$ states observed above 2.7 MeV in ^{128}Te, no ground-state decay is observed for the level at 2712.4 keV, and no decays to the 2^+_1 state are observed for the 2997.5- and 3105.1-keV levels. Levels at 2763.9 and 3185.5 keV have lifetimes of 24(3) and 72^{+12}_{-11} fs, respectively, and ground-state branches similar to those observed in ^{122,124}Te. The 2763.9-keV γ ray dominates the spectrum of ^{128}Te in the energy region shown in Fig. 6, much like ground-state transitions from candidate QOC states in ^{122,124,126}Te. The $B(E1)$ value for the ground-state decay agrees will with the QPM value in panel (c) of Fig. 6. The 2763.9-keV level also decays into the 2^+_2 state which is predicted by *spdf*-IBM-2 calculations [72], but the important decay into the 3^-_1 state is not observed; this was also the case in (n,n',γ) measurements on ^{122,124}Te. The two-phonon decay $1^-_1 \rightarrow 0^+_1$ is predicted to have a strength comparable to $B(E1; 3^-_1 \rightarrow 2^+_1)$ [73], but the experimental $B(E1; 3^-_1 \rightarrow 2^+_1) = 3.1(3) \times 10^{-4}$ e^2 fm^2 differs by about a factor of three for the 2763.9-keV level. An additional problem with attributing QOC character to this level is that its energy is about 475 keV below the experimentally expected QOC energy of 3237 keV; this difference is rather large compared to other identified QOC 1^--state candidates in the Te nuclei.

The 3185.6-keV level is the other possible 1^- state observed in these measurements with similar decay branches to the ground and first excited states, although the decay to the 2^+_1 state is tentative. The maximum $B(E1)$ for the ground-state transition for this level is more than a factor of three smaller than that predicted by QPM calculations for the 1^- QOC state [25]. Based on the very systematic behavior of the energy [25,70,74] of the 1^- QOC state in nearby isotopic chains, the 3185.6-keV level is, however, the best candidate, as it lies about 50 keV below the $E(2^+_1) + E(3^-_1)$ energy. Clearly, the parities need to be determined for these levels.

QOC 3^- state. The 3139.9 keV $J = 3$ level has a tentative decay into the 3^-_1 state and is the best candidate for the 3^- QOC state. This level is also observed to decay into both of the $2^+_{1,\mathrm{MS}}$ levels. Unfortunately, no lifetime was obtained for this level and so it was not possible to make the comparison with important transition rates. The octupole excitation strength was observed in proton-scattering measurements [4,7] to be split between levels at 2490(10) and 3160(20) keV in ^{128}Te; the octupole strength of the higher 3^- state was observed to be 25% of the 3^-_1 [7]. The results from those dated proton scattering measurements support the negative-parity assignment of this level and its QOC character, provided the

level seen at 3160(20) keV corresponds to the 3139.9-keV level observed in the $(n,n'\gamma)$ measurements.

The coincidence gate set on the 3_1^- to 2_1^+ transition in ^{128}Te reveals that few transitions feed this level, at least down to the detection threshold and energy threshold of the coincidence measurements performed here. No other reasonable candidates for QOC states are observed, which may indicate that they are located above the energy range studied in these $(n,n'\gamma)$ measurements. Most of the low-lying negative-parity states are observed to decay into the 5_1^- level discussed below and are thought to be dominated by few-particle configurations.

C. Quasiparticle excitations

1. Lowest 2-quasiparticle $J^\pi = 1^+$ state

The lowest spin-1 levels observed in $^{122-130}$Te are 1^+ levels at about 2 MeV, as shown in Fig. 7; in ^{128}Te, $E(1_1^+) = 2217.9$ MeV. These levels were previously identified as the first $2qp$ $J = 1$ states in $^{122-130}$Te; furthermore, the $\pi^2(3s_{1/2}, 2d_{3/2})$ configuration was considered to be the most important configuration due to the low energies of the $\frac{1}{2}^+$ and $\frac{3}{2}^+$ levels in the neighboring odd-mass Te nuclei [20]. The particle-core coupling model calculations for ^{128}Te discussed above place the first 1^+ level at 2.37 MeV, about the observed energy, and indicate that the $\pi^2(1g_{7/2}, 2d_{5/2})$ $2qp$ configuration is the largest component of the wave function (46%); the next-largest component contains the $\hbar\omega_2 \otimes \pi^2(1g_{7/2})^2$ configuration, which accounts for about 13% of the strength in ^{128}Te. The $s_{1/2}$ configuration is in no component containing more than 5% of the PCM model wave function for this level. The energies [75–81] of the $\frac{5}{2}^+$ and $\frac{7}{2}^+$ excited states, where identified, remain more constant in energy for $^{119-131}$Te than do the $\frac{1}{2}^+$ and $\frac{3}{2}^+$ state energies, at least until ^{131}Te; these odd-mass state energies

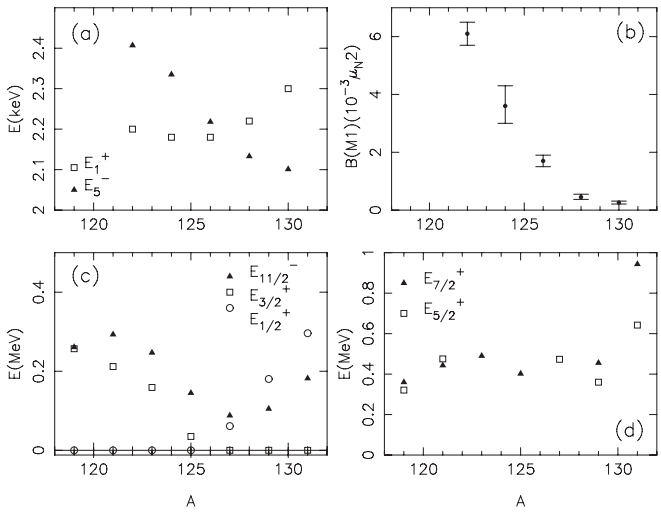

FIG. 7. (a) Energies of the 1_1^+ and 5_1^- states in $^{122-130}$Te. (b) The $B(M1; 1_1^+ \rightarrow 0_1^+)$ values for 1^+ level decays in (a). Panels (c) and (d) give the excitation energies of states in the neighboring odd-mass Te nuclei from Refs. [75–81].

are shown in Fig. 7. This property could explain the small variation in the energy of the 1_1^+ level across the isotopic chain, although the $\frac{5}{2}^+$ and $\frac{7}{2}^+$ excited states are not identified in all the odd-mass Te nuclei of interest, nor do these states necessarily have large spectroscopic factors [75–81]. The observed $B(M1)$ and $B(E2)$ values of the decays from these 1^+ levels support their noncollective interpretation. The energy of the 1^+ levels in $^{122-130}$Te and and $B(M1; 1_1^+ \rightarrow 0_1^+)$ are shown in Figs. 7(a) and 7(b), respectively. The $B(M1)$ values are all relatively small, but there is an increase in $M1$ strength in moving away from the $N = 82$ shell closure. Particle-core coupling model calculations for ^{128}Te with $g_l = 0.5$ predict $B(M1; 1_1^+ \rightarrow 0_1^+) = 0.36 \times 10^{-2}\mu_N^2$, which is an order of magnitude larger than that observed experimentally, while PCM calculations with $g_l = 1.0$ give $B(M1; 1_1^+ \rightarrow 0_1^+) = 0.30 \times 10^{-5}\mu_N^2$, which is about two orders of magnitude too small. This level is not in the IBM-2 model space, so no comparisons can be made with predictions from that model.

2. 5_1^- Level

Across the Te isotopic chain, 5^- and 7^- $2qp$ states occur at 2 to 3 MeV in excitation. The most likely configurations for these states are the two-neutron quasiparticle states $(h_{\frac{11}{2}}, s_{\frac{1}{2}})_{5^-}$ and $(h_{\frac{11}{2}}, d_{\frac{3}{2}})_{7^-}$ [3]; this suggestion is supported experimentally by hindered $E1$ transitions from these states to the 6_1^+ state because of the proton $2qp$ character [82] of the latter. These 5_1^- levels were studied using (p,p') [7] and (p,t) reactions [5,9], and the observed enhanced cross sections of the population of these states as a function of neutron number led to the conclusion that they are predominantly, although not purely, neutron $2qp$ excitations. This conjecture is further supported by a shell-model analysis in which the 5_1^- states in ^{122,126,128,130}Te are described as being formed from the promotion of a neutron from an $s_{\frac{1}{2}}$ into an $h_{\frac{11}{2}}$ orbital, such that the final state is described as an $(s_{\frac{1}{2}}^1, h_{\frac{11}{2}}^{m+1})$ configuration, where $m = 0, 4, 6, 8$ for ^{122}Te, ^{126}Te, ^{128}Te, and ^{130}Te, respectively [8]. The energies of these states are expected to decrease as the Te isotopes become more neutron rich and the population of these states is expected to compete with collective states of the same spin and parity. The energy behavior expected for the lowest 5^- state is observed across the Te isotopic chain and is well established [3,7,8]. These new results for ^{128}Te show the importance of the 5_1^- state in the *decays* of higher-lying states. Similar behavior is observed in ^{126}Te, but not in ^{122,124}Te. Few lifetimes for the states decaying into the 5_1^- state were measurable using DSAM techniques, which strongly supports the noncollective interpretation of these excitations. The PCM calculations, which predict the energy of the proton $2qp$ 1^+ state within about 100 keV, put the energy of the first 5^- state at over 3.5 MeV, signifcantly above the observed energy in ^{128}Te. The leading configuration in the PCM wave function for this state is $\hbar\omega_3 \otimes \pi^2(1g_{7/2})^2$, which differs from earlier calculations [8]. For both the 1_1^+ and the 5_1^- states, the $3s_{1/2}$ single-particle state does not contribute significantly to the PCM wave function; however, the trend of the energy of the 5_1^- level from $^{120-130}$Te closely follows the behavior of the

$\frac{11}{2}^-$ state in the odd-mass Te nuclei, as can be seen in Fig. 7. This behavior supports the importance of the $\nu^2(1h_{11/2},3s_{1/2})$ neutron configurations in the structure of the 5^- states. These two-neutron excitations are not well represented in the PCM model space, which emphasizes two proton particles coupled to collective core excitations.

VI. SUMMARY

The level scheme and decay characteristics of levels in ^{128}Te to 3.3 MeV in excitation have been investigated using the $(n,n'\gamma)$ reaction. Forty-four new levels and approximately 90 new transitions were identified. Additionally, branching ratios, multipole-mixing ratios, spins, and lifetimes were deduced for many transitions and states from γ-ray excitation functions, angular distributions, $\gamma\gamma$ coincidences, and Doppler shifts.

The low-lying positive-parity levels in ^{128}Te were compared to IBM-1, IBM-2, and PCM calculations. Intruder states were investigated by comparing experimental levels with calculations performed using the IBM-2 with intruder-state mixing. These calculations revealed that the intruder states were predicted relatively high in energy and could not be easily identified in the data. IBM-2 calculations reproduced the energies and spins of many low-lying states, as did the IBM-1 calculations, but with less success than the PCM calculations. The PCM model also better described the observed electromagnetic transition rates, as long as g_l was reduced from the free-proton value.

Levels were found that exhibited some two-phonon MS characteristics for the full quintuplet of states formed from $2^+_{1,S} \otimes 2^+_{1,\mathrm{MS}}$ excitations. The fragmentation of MS strength in the $2^+_{1,\mathrm{MS}}$ states, however, was observed to lead to a fragmentation of MS strength in the higher-lying states and to a lack of $M1$ strength in any specific state.

Two candidates were identified for the 1^- QOC state in ^{128}Te. One of these states had decay characteristics consistent with those expected for a QOC state, but it occurs 450 keV below the expected energy, which is unusual for nuclei in this mass region. The other candidate is at about the expected energy, but its decay characteristics are not consistent with those expected for QOC states. The only other QOC state candidate is a $J = 3$ state at 3139.9 keV. Candidates for other members of the quintuplet were not identified, as they may be higher than 3.3 MeV in excitation energy.

Finally, $2qp$ 1^+ and 5^- excitations were examined with PCM model calculations and by looking at excitations in odd-mass Te isotopes. The former can be well explained by a model that includes two proton particles coupled to a collective vibrational core. The 5^- state, which was previously identified as predominantly a two-neutron excitation, is not well described by PCM calculations. Additionally, this 5^- level was found to be very important in the decay of higher-lying states, which appear to be few-particle excitations based on their lifetimes and decay properties.

ACKNOWLEDGMENTS

This material is based on work supported by the National Science Foundation under Grants No. PHY-9901508, No. PHY-9971711, No. PHY-0098813, and No. PHY-0956310. Additionally, we would like to thank the O'Hara Foundation at the University of Dallas for summer support for students. The authors would also like to express their sincere appreciation to Professor Emeritus Marcus T. McEllistrem, Professor Emeritus John Wood, and Professor Jan Jolie for fruitful discussions during the analysis and manuscript preparation and to accelerator engineer Harvey Baber for sharing his expertise and time to help us complete this project.

[1] J. A. Cookson and W. Darcey, Nucl. Phys. **62**, 326 (1965).
[2] V. Lopac, Nucl. Phys. A **155**, 513 (1970).
[3] A. Kerek, Nucl. Phys. A **176**, 466 (1971).
[4] M. Matoba, M. Hyakutake, S. Nakamura, T. Katayama, T. Tonai, K. Yagi, K. Sato, and Y. Aoki, Phys. Lett. B **44**, 159 (1973).
[5] M. Matoba, M. Hyakutake, K. Yagi, Y. Aoki, and C. Rangacharyulu, J. Phys. Soc. Jpn. **36**, 1468 (1974).
[6] T. Izumoto, Y. Aoki, C. Rangacharyulu, T. Yagi, M. Matoba, and M. Hyakutake, Phys. Lett. B **57**, 17 (1975).
[7] M. Matoba, M. Hyakutake, K. Yagi, and Y. Aoki, Nucl. Phys. A **237**, 260 (1975).
[8] P. Nesci, R. Smith, K. Amos, and H. V. Geramb, Aust. J. Phys. **28**, 659 (1975).
[9] M. Matoba, M. Hyakutake, K. Yagi, Y. Aoki, and C. Rangacharyulu, Nucl. Phys. A **261**, 223 (1976).
[10] L. I. Govor, A. M. Demidov, and M. M. Komkov, Yad. Fiz. **29**, 1425 (1979) [Sov. J. Nucl. Phys. **29**, 731 (1979)].
[11] J. J. Van Ruyven, W. H. A. Hesselink, J. Akkermans, P. Van Nes, and H. Verheul, Nucl. Phys. A **380**, 125 (1982).
[12] M. Sambataro, Nucl. Phys. A **380**, 365 (1982).
[13] A. Giannatiempo, A. Nannini, A. Perego, and P. Sona, Phys. Rev. C **36**, 2528 (1987).
[14] R. Nojarov and A. Faessler, J. Phys. G **13**, 337 (1987).
[15] A. Subber, W. D. Hamilton, P. Park, and K. Kumar, J. Phys. G **13**, 161 (1987).
[16] J. Rikovska, N. J. Stone, and W. B. Walters, Phys. Rev. C **36**, 2162 (1987).
[17] P. M. Walker, C. J. Ashworth, I. S. Grant, V. R. Green, J. Rikovska, T. L. Shaw, and N. J. Stone, J. Phys. G: Nucl. Phys. **13**, L195 (1987).
[18] A. M. Demidov, L. I. Govor, V. A. Kurkin, I. V. Mikhailov, S. Yu. Araddad, J. M. Rateb, and S. M. Zlitni, Sov. J. Nucl. Phys. **47**, 571 (1988).
[19] J. Rikovska, N. J. Stone, P. M. Walker, and W. B. Walters, Nucl. Phys. A **505**, 145 (1989).
[20] S. A. Berendakov, L. I. Govor, A. M. Demidov, and I. V. Mikhailov, Yad Fiz. **52**, 609 (1990) [Sov. J. Nucl. Phys. **52**, 389 (1990)].
[21] C. S. Lee, J. A. Cizewski, D. Barker, R. Tanczyn, G. Kumbartzki, J. Szczepanski, J. W. Gan, H. Dorsett, R. G. Henry, and L. P. Farris, Nucl. Phys. A **528**, 381 (1991).

[22] J. A. Cizewski, L. A. Bernstein, R. G. Henry, H. Q. Jin, C. S. Lee, and W. Younes, in *Proceedings of the 8th International Symposium on Capture Gamma-Ray Spectroscopy and Related Topics*, edited by J. Kern (World Scientific Press, Singapore, 1993), pp. 328–334.

[23] R. Georgii, T. von Egidy, J. Klora, H. Lindner, U. Mayerhofer, J. Ott, W. Schauer, P. von Neumann-Cosel, A. Richter, C. Schlegel, R. Schulz, V. A. Khitrov, A. M. Sukhovoj, A. V. Vojnov, J. Berzins, V. Bondarenko, P. Prokofjev, L. J. Simonova, M. Grinberg, and Ch. Stoyanov, Nucl. Phys. A **592**, 307 (1995).

[24] J. Ott, C. Doll, T. von Egidy, R. Georgii, M. Grinberg, W. Schauer, R. Schwengner, and H.-F. Wirth, Nucl. Phys. A **625**, 598 (1997).

[25] R. Schwengner *et al.*, Nucl. Phys. A **620**, 277 (1997).

[26] N. Warr, S. Drissi, P. E. Garrett, J. Jolie, J. Kern, H. Lehman, S. J. Mannanal, and J.-P. Vorlet, Nucl. Phys. A **636**, 379 (1998), and references therein.

[27] W. Schauer, C. Doll, T. von Egidy, R. Georgii, J. Ott, H.-F. Wirth, A. Gollwitzer, G. Graw, R. Hertenberger, B. Valnion, M. Grinberg, and Ch. Stoyanov, Nucl. Phys. A **652**, 339 (1999), and references therein.

[28] E. Guliyev, A. A. Kuliev, P. von Neumann-Cosel, and A. Richter, Phys. Lett. B **532**, 173 (2002).

[29] J. R. Vanhoy, R. T. Coleman, K. A. Crandell, S. F. Hicks, B. A. Sklaney, M. M. Walbran, N. V. Warr, J. Jolie, F. Corminboeuf, L. Genilloud, J. Kern, J.-L. Schenker, and P. E. Garrett, Phys. Rev. C **68**, 034315 (2003).

[30] A. M. Demidov, L. I. Gover, V. A. Kurkin, and I. V. Mikhailov, Phys. At. Nucl. **67**, 1884 (2004).

[31] J. R. Vanhoy, J. A. Tanyi, K. A. Crandell, T. H. Churchill, S. F. Hicks, M. C. Burns, P. A. Roddy, N. V. Warr, T. B. Brown, and S. R. Lesher, Phys. Rev. C **69**, 064323 (2004).

[32] S. F. Hicks, G. K. Alexander, C. A. Aubin, M. C. Burns, C. J. Collard, M. M. Walbran, J. R. Vanhoy, E. Jensen, P. E. Garrett, M. Kadi, A. Martin, N. Warr, and S. W. Yates, Phys. Rev. C **71**, 034307 (2005).

[33] S. F. Hicks, J. R. Vanhoy, and S. W. Yates, Phys. Rev. C **78**, 054320 (2008).

[34] S. Pascu, N. V. Zamfir, Gh. Căta-Danil, and N. Mărginean, Phys. Rev. C **81**, 054321 (2010).

[35] N. Turkan and I. Maras, Math. Comput. Appl. **16**, 467 (2011).

[36] F. Iachello, Phys. Rev. Lett. **53**, 1427 (1984).

[37] P. Vogel and L. Kocbach, Nucl. Phys. A **176**, 33 (1971).

[38] N. Takaoka and K. Ogata, Z. Naturforsch. **21a**, 84 (1966).

[39] B. Pontecorvo, Phys. Lett. B **26**, 630 (1968).

[40] E. W. Hennecke and O. K. Manuel, Phys. Rev. C **11**, 1378 (1975).

[41] Tomás R. Rodríguez and Gabriel Martínez-Pinedo, Phys. Rev. Lett. **105**, 252503 (2010).

[42] C. A. McGrath, M. F. Villani, P. E. Garrett, and S. W. Yates, Nucl. Instrum. Methods Phys. Res., Sect. A **421**, 458 (1999).

[43] P. E. Garrett, N. Warr, and S. W. Yates, J. Res. Natl. Inst. Stand. Technol. **105**, 141 (2000), and references therein.

[44] M. Kanbe and K. Kitao, Nucl. Data Sheets **94**, 227 (2001).

[45] E. Sheldon and D. M. van Patter, Rev. Mod. Phys. **38**, 143 (1966).

[46] R. W. Harper, T. W. Godfrey, and J. L. Weil, Phys. Rev. C **26**, 1432 (1982).

[47] T. Belgya, G. Molnár, and S. W. Yates, Nucl. Phys. A **607**, 43 (1996).

[48] K. B. Winterbon, Nucl. Phys. A **246**, 293 (1975).

[49] A. Aprahamian, D. S. Brenner, R. F. Casten, R. L. Gill, and A. Piotrowski, Phys. Rev. Lett. **59**, 535 (1987).

[50] M. Kadi, N. Warr, P. E. Garrett, J. Jolie, and S. W. Yates, Phys. Rev. C **68**, 031306(R) (2003).

[51] J. Kumpulainen, R. Julin, J. Kantele, A. Passoja, W. H. Trzaska, E. Verho, J. Vaaramaki, D. Cutoiu, and M. Ivascu, Phys. Rev. C **45**, 640 (1992).

[52] D. C. Radford, A. Galindo-Uribarri, G. Hackman, and V. P. Janzen, Nucl. Phys. A **557**, 311 (1993).

[53] M. Schimmer, R. Wirowski, S. Albers, G. Bohm, A. Dewald, A. Gelberg, and P. von Brentano, Z. Phys. A **338**, 117 (1991).

[54] E. S. Paul *et al.*, Phys. Rev. C **50**, 698 (1994).

[55] O. Scholten, *Computational Nuclear Structure Physics I: Nuclear Structure*, edited by K. Langanke, J. A. Maruhn, and S. E. Koonin (Springer-Verlag, Berlin, 1991), p. 88.

[56] P. D. Duval and B. R. Barrett, Nucl. Phys. A **376**, 213 (1982).

[57] T. Otsuka and N. Yoshida, Japanese Atomic Energy Research Institute Report 85-094, 1985.

[58] P. Van Isacker, K. Keyde, J. Jolie, and A. Sevrin, Ann. Phys. **171**, 253 (1986).

[59] A. Giannatiempo, G. Maino, A. Nannini, and P. Sona, Phys. Rev. C **48**, 2657 (1993).

[60] J. R. Vanhoy, J. M. Anthony, B. M. Haas, B. H. Benedict, B. T. Meehan, Sally F. Hicks, C. M. Davoren, and C. L. Lundstedt, Phys. Rev. C **52**, 2387 (1995).

[61] K. Heyde and P. J. Brussard, Nucl. Phys. A **104**, 81 (1967).

[62] E. Degrieck and G. Van den Berghe, Nucl. Phys. A **231**, 141 (1974).

[63] J. Copnell, S. J. Robinson, J. Jolie, and K. Heyde, Phys. Rev. C **46**, 1301 (1992).

[64] L. Y. Jia, H. Zhang, and Y. M. Zhao, Phys. Rev. C **75**, 034307 (2007).

[65] N. Pietralla, C. Fransen, A. Gade, N. A. Smirnova, P. von Brentano, V. Werner, and S. W. Yates, Phys. Rev. C **68**, 031305(R) (2003).

[66] N. Pietralla, C. Fransen, D. Belic, P. von Brentano, C. Frießner, U. Kneissl, A. Linnemann, A. Nord, H. H. Pitz, T. Otsuka, I. Schneider, V. Werner, and I. Wiedenhöver, Phys. Rev. Lett. **83**, 1303 (1999).

[67] N. Pietralla, C. Fransen, P. von Brentano, A. Dewald, A. Fitzler, C. Frießner, and J. Gableske, Phys. Rev. Lett. **84**, 3775 (2000).

[68] S. R. Lesher, C. J. McKay, M. Mynk, D. Bandyopadhyay, N. Boukharouba, C. Fransen, J. N. Orce, M. T. McEllistrem, and S. W. Yates, Phys. Rev. C **75**, 034318 (2007).

[69] N. Pietralla, P. von Brentano, and A. F. Lisetskiy, Prog. Part. Nucl. Phys. **60**, 225 (2008).

[70] H. von Garrel *et al.*, Phys. Rev. C **73**, 054315 (2006).

[71] C. Kohstall, D. Belic, P. von Brentano, C. Fransen, A. Gade, R.-D. Herzberg, J. Jolie, U. Kneissl, A. Linnemann, A. Nord, N. Pietralla, H. H. Pitz, M. Scheck, F. Stedile, V. Werner, and S. W. Yates, Phys. Rev. C **72**, 034302 (2005).

[72] N. A. Smirnova, N. Pietralla, T. Mizusaki, and P. Van Isacker, Nucl. Phys. A **678**, 235 (2000).

[73] N. Pietralla, Phys. Rev. C **59**, 2941 (1999).

[74] U. Kneissl, N. Pietralla, and A. Zilges, J. Phys. G **32**, R217 (2006).

[75] D. M. Symochko, E. Browne, and J. K. Tuli, Nucl. Data Sheets **110**, 2945 (2009).

[76] S. Ohya, Nucl. Data Sheets **111**, 1619 (2010).

[77] S. Ohya, Nucl. Data Sheets **102**, 547 (2004).
[78] J. Katakura, Nucl. Data Sheets **112**, 495 (2011).
[79] A. Hashizume, Nucl. Data Sheets **112**, 1647 (2011).
[80] Y. Tendow, Nucl. Data Sheets **77**, 631 (1996).
[81] Yu. Khazov, I. Mitropolsky, and A. Rodionov, Nucl. Data Sheets **107**, 2715 (2006).
[82] J. C. Soares, P. Herzog, H. Hübel, A. Kluge, and W. Thomas, Nucl. Phys. A **247**, 247 (1975).